

## MIT Open Access Articles

*Comparison of neutron organ and effective dose coefficients for PIMAL stylized phantom in bent postures in standard irradiation geometries*

The MIT Faculty has made this article openly available. **Please share** how this access benefits you. Your story matters.

**As Published:** <https://doi.org/10.1007/s00411-018-0751-8>

**Publisher:** Springer Berlin Heidelberg

**Persistent URL:** <https://hdl.handle.net/1721.1/131409>

**Version:** Author's final manuscript: final author's manuscript post peer review, without publisher's formatting or copy editing

**Terms of Use:** Article is made available in accordance with the publisher's policy and may be subject to US copyright law. Please refer to the publisher's site for terms of use.



1 **Original Paper**

2

3 K. Bales, S. Dewji, E. Sanchez

4

5 **Comparison of neutron organ and effective dose coefficients for PIMAL**  
6 **stylized phantom in bent postures in standard irradiation geometries**

7

8 K. Bales, S. Dewji (✉), E. Sanchez  
9 Oak Ridge National Laboratory, Center for Radiation Protection Knowledge, Oak Ridge,  
10 TN, USA  
11 E-mail: dewjisa@ornl.gov

12 K. Bales  
13 University of Tennessee – Knoxville, Department of Nuclear Engineering, Knoxville,  
14 TN, USA

15 E. Sanchez  
16 Massachusetts Institute of Technology, Department of Nuclear Science and Engineering,  
17 Cambridge, MA, USA

18

19 Notice: This manuscript has been authored by UT-Battelle, LLC, under Contract No. DE-  
20 AC0500OR22725 with the U.S. Department of Energy. The United States Government  
21 retains and the publisher, by accepting the article for publication, acknowledges that the  
22 United States Government retains a non-exclusive, paid-up, irrevocable, world-wide  
23 license to publish or reproduce the published form of this manuscript, or allow others to  
24 do so, for the United States Government purposes. The Department of Energy will  
25 provide public access to these results of federally sponsored research in accordance with  
26 the DOE Public Access Plan (<http://energy.gov/downloads/doe-public-access-plan>).

27

28 **Abstract** Neutron dose coefficients for standard irradiation geometries have been  
29 reported in International Commission on Radiological Protection (ICRP) Publication 116  
30 for the ICRP Publication 110 adult reference phantoms. In the present work, organ and  
31 effective dose coefficients have been calculated for a receptor in both upright and  
32 articulated (bent) postures representing more realistic working postures exposed to a  
33 mono-energetic neutron radiation field. This work builds upon prior work by Dewji and  
34 co-workers comparing upright and bent postures for exposure to mono-energetic photon  
35 fields. Simulations were conducted using the Oak Ridge National Laboratory's  
36 articulated stylized adult phantom, "Phantom with Moving Arms and Legs" (PIMAL)  
37 software package, and the Monte Carlo N-Particle (MCNP) version 6.1.1 radiation  
38 transport code. Organ doses were compared for the upright and bent (45° and 90°)  
39 phantom postures for neutron energies ranging from  $1 \cdot 10^{-9}$  to 20 MeV and the ICRP  
40 Publication 116 external exposure geometries – antero-posterior (AP), postero-anterior  
41 (PA), and left and right lateral (LLAT, RLAT). Using both male and female phantoms,  
42 effective dose coefficients were computed using ICRP Publication 103 methodology. The  
43 resulting coefficients for articulated phantoms were compared to those of the upright  
44 phantom. Computed organ and effective dose coefficients are discussed as a function of  
45 neutron energy, phantom posture, and source irradiation geometry. For example, it is  
46 shown here that for the AP and PA irradiation geometries, the differences in the organ  
47 coefficients between the upright and bent posture become more pronounced with  
48 increasing bending angle. In the AP geometry, the brain dose coefficients are expectedly  
49 higher in the bent postures than in the upright posture, while all other organs have lower  
50 dose coefficients, with the thyroid showing the greatest difference. Overall, the effective  
51 dose estimated for the upright phantom is more conservative than that for the articulated  
52 phantom, which may have ramifications in the estimation or reconstruction of radiation  
53 doses.

54

## 55 **Introduction**

56 Estimation of radiation dose in the human body is a complex problem necessitating the  
57 use of computational modeling of the exposure geometry and mathematical  
58 representation of the human body by means of anthropomorphic phantoms. Using the  
59 methodology in the International Commission on Radiological Protection (ICRP)  
60 Publication 103 (ICRP 2007), the equivalent dose coefficients calculated in organs and  
61 tissues of the reference male and female phantoms are used to determine the effective  
62 dose. A revision of the dose coefficients found in ICRP Publication 74 (ICRP 1996) has  
63 been released in ICRP Publication 116, employing the ICRP Publication 110 reference  
64 adult phantoms (ICRP 2009) for the standard irradiation source geometries: antero-  
65 posterior (AP), postero-anterior (PA), left and right lateral (LLAT, RLAT), and isotropic  
66 (ISO) radiation fields. While ICRP Publication 116 tabulates dose coefficients for the  
67 exposure source geometries employed in the present work, those ICRP coefficients were  
68 determined using computational phantoms positioned in an upright position derived from  
69 computed tomography (CT) scans in the supine position, published as the ICRP reference  
70 adult male and female phantoms in ICRP Publication 110 (ICRP 2009).

71 Most dose reconstruction studies have been performed using an upright phantom,  
72 which may not provide a good dose estimate for the body postures likely to be  
73 encountered in an occupational setting. In addition, real-world exposures do not involve  
74 parallel mono-energetic beams or isotropic fields; therefore, this work focuses on the  
75 effect of body posture. Some works have already argued that posture is critical for dose  
76 reconstruction involving a seated subject (Dewji et al. 2014, Han et al. 2014, Alves et al.  
77 2016). There are only few studies in which phantoms in a specific working posture have  
78 been explored for dose reconstruction purposes and fewer have been explored with a  
79 focus on the neutron source variable. Akkurt et al (2009) investigated dose received by a  
80 glovebox worker in a realistic posture using a phantom with extended arms (Akkurt and  
81 Eckerman 2007) for both a neutron spectrum, as well as a clean weapons-grade  
82 plutonium source. Additionally, Vasquez et al. (2014) recreated postures observed from a  
83 motion capture system to more accurately assess doses received by two workers in the  
84 criticality accident that took place in Tokai-Mura, Japan in 1999.

85           In the work explored here, dose calculations were performed using upright and  
86 bent phantom postures to analyze the differences in dose due to these various postures in  
87 standard irradiation mono-energetic neutron fields. This work builds upon prior work by  
88 Dewji et al. (2017), which represents the photon counterpart of the work conducted here.  
89 Both these works explore the role of body posture in dose reconstruction for four of the  
90 irradiation geometries of ICRP Publication 116 (2010).

91

## 92 **Methods**

### 93 PIMAL phantom

94 Mathematical models of the human body models have almost exclusively been created in  
95 a rigid, upright posture (Xu 2014). The “**Phantom wIth Moving Arms and Legs**”  
96 (PIMAL) software developed by Oak Ridge National Laboratory employs a graphical  
97 user interface (GUI) to allow for a customizable geometry of the phantom (Akkurt and  
98 Eckerman 2007). Phantom geometry can be described using slider bars or a textbox to  
99 input joint angle for the shoulder, elbow, knee and hip joints. The GUI, captured in prior  
100 work by Dewji et al. (2017), allows the user to visualize and adjust the position of the  
101 arms and legs. PIMAL has been updated to include two separate reference stylized male  
102 and female phantoms (Dewji and Hiller, 2016) with tissue compositions and densities  
103 from ICRP Publication 89 (ICRP 2002), and to include the ICRP 110 reference voxel  
104 phantoms (ICRP 2009); however, these phantoms remain in a static upright position.  
105 Prior work by Bellamy et al. (2016) and Hiller and Dewji (2017) compare, in detail, the  
106 anatomical differences between reference adult voxel and stylized phantom in an external  
107 air submersion cloud of mono-energetic photons for the updated ORNL stylized  
108 phantoms. In these studies, the voxel resolution of thin-walled organs, intra-organ  
109 position, and elaboration of skeletal response functions for bone surface and active  
110 marrow dosimetry contributed the greatest variation in organ and effective dose  
111 coefficients for external photon irradiation sources. The differences between the upright  
112 voxel and stylized phantoms are detailed in these studies, and the reader is referred to  
113 these works for comparisons.

114 After the phantom has been positioned to the user's specifications and the  
115 parameters have been set, PIMAL creates and executes an input file for the Monte Carlo  
116 N-Particle (MCNP) radiation transport code. Organ dose coefficients may then be  
117 extracted from the MCNP output files. The simulation part of PIMAL allows the user to  
118 set various parameters for the simulation: the mode specifies neutron and/or photon  
119 sources, the source energy allows the user to set external and internal sources for mono-  
120 energetic neutron/photon energy, external source geometries allow the user to select a  
121 point source with user-specified X, Y, Z coordinates, or source geometries listed in ICRP  
122 Publication 116, internal source geometries allow organ volume sources to be set in the  
123 body, and the MCNP Input Generation and Execution allows the code to be run within  
124 PIMAL, producing an organ dose table that can be exported as an ASCII file. The MCNP  
125 output file is also saved and can be used to analyze the derived dose coefficients in detail.

126 In the present work, the organ and effective dose coefficients for the bent posture  
127 are compared to those for an upright posture, and the coefficients for the upright posture  
128 were compared to those tabulated in ICRP Publication 116. PIMAL was used to orient  
129 the torso of male and female phantoms with repositioned arms and legs at 45° and 90°  
130 from the vertical axis (half and full bent postures) to represent the effects of articulated  
131 postures in theoretical exposure fields (Fig. 1).



132

133 **Fig 1** The upright, half-bent (45°), and full-bent (90°) side views taken from the PIMAL  
134 4.1.0 GUI for the stylized phantom.

135 Monte Carlo simulations

136 The 6.1.1 version of the MCNP radiation transport code (Pelowitz et al. 2014) was used  
137 to calculate the absorbed doses in each of the organs. Using both male and female  
138 stylized phantoms represented in PIMAL, organ dose data was computed using MCNP  
139 for each of the five irradiation geometries using upright, half-bent (45°), and full-bent  
140 phantoms (90°). These simulations were conducted for the following range of mono-  
141 energetic neutron energies for each case:  $1 \cdot 10^{-9}$  to 20 MeV. A 200 cm × 200 cm plane  
142 was used for each irradiation geometry, placed 1 m from the center of the PIMAL  
143 phantom. The simulations were run in a vacuum.

144 Organ doses were computed using the MCNP +F6 collision heating tally in  
145 MeV/g. Doses for active marrow and bone surface were estimated by applying the  
146 skeletal response functions of ICRP Publication 116 (ICRP 2010) to the MCNP F4 tally  
147 in particles/cm<sup>2</sup> in the skeletal regions outside of PIMAL. All simulations were run until  
148 statistical errors converged within < 10% for most neutron energies.

149 Effective dose calculations

150 Using the organ dose coefficients provided from the MCNP simulations, the effective  
151 dose coefficient,  $E$ , was calculated using the methodology of ICRP Publication 103  
152 (2007). Effective dose coefficient was determined as follows:

153 
$$E = \sum_T w_T \left[ \frac{H_T^M + H_T^F}{2} \right] \quad (1)$$

154 where  $H_T^M$  is the equivalent dose coefficient in organ/tissue  $T$  for the male phantom,  $H_T^F$  is  
155 the equivalent dose coefficient in organ/tissue  $T$  for the female phantom, and  $w_T$  is the  
156 tissue weighting factor for organ/tissue  $T$ . The tissue weighting factors defined in ICRP  
157 Publication 103 are shown in Table 1.

158

159 **Table 1** ICRP Publication 103 tissue weighting factors (International Commission on  
 160 Radiological Protection 2007).

Tissue	$w_T$	$\sum w_T$
Bone-marrow (red), Colon, Lung, Stomach, Breast, Remainder tissues*	0.12	0.72
Gonads	0.08	0.08
Bladder, Esophagus, Liver, Thyroid	0.04	0.16
Bone surface, Brain, Salivary glands, Skin	0.01	0.04
Total		1.00

\*Remainder tissues: Adrenals, Extrathoracic region, Gall bladder, Heart, Kidneys, Lymphatic nodes, Muscle, Oral mucosa, Pancreas, Prostate (M), Small intestine, Spleen, Thymus, Uterus/cervix (F)

161

162 Male and female equivalent dose coefficients are computed as:

163 
$$H_T = \sum_R w_R D_{T,R} \quad (2)$$

164 where  $w_R$  is the radiation weighting factor and  $D_{T,R}$  is the absorbed dose from radiation  $R$   
 165 to organ/tissue  $T$ . For this work, the radiation weighting factors for neutrons from ICRP  
 166 Publication 103 (2007) are employed:

167 
$$w_R = \begin{cases} 2.5 + 18.2e^{-[\ln(E_n)]^2/6}, & E_n < 1 \text{ MeV} \\ 5.0 + 17.0e^{-[\ln(2E_n)]^2/6}, & 1 \text{ MeV} \leq E_n \leq 50 \text{ MeV} \\ 2.5 + 3.25e^{-[\ln(0.04E_n)]^2/6}, & E_n > 50 \text{ MeV} \end{cases} \quad (3)$$

168 where  $w_R$  is a function of neutron energy,  $E_n$ .



169 Since neutrons are uncharged, energy is imparted through collisions and  
170 absorption with nuclides to tissues by secondary particles; i.e., liberated charged particles  
171 and photons. Element composition and density of the tissues can have an impact on the  
172 imparted energy. The photon dose contribution is strongly dependent on neutron energy.  
173 For example, at low energies (e.g. thermal energy), the contribution of neutron-liberated  
174 photons dominates the absorbed dose. The radiation weighting factors, found in ICRP  
175 Publication 103 (2007) and shown in Fig. 2 reflect the relative energy deposition via  
176 neutron interactions. Equivalent dose coefficients were computed using Eq. 2 and  
177 employing the radiation weighting factors found in Eq. 3. The MCNP F4 tally used to  
178 determine dose rates for the active marrow and endosteum separated the neutron and  
179 photon contributions, while the dose rates determined for the other organs and tissues did  
180 not. The two were added together to determine the total dose for each irradiation  
181 geometry, energy, and posture. The energy-dependent neutron weighting factors were  
182 then applied to the total dose from the neutrons and secondary particles for the skeletal  
183 organs.

184

## 185 **Results and discussion**

### 186 Organ absorbed dose ratios

187 The sex-averaged organ absorbed dose coefficients for the bent postures were compared  
188 to the upright posture. These calculated ratios are found in Table 2 for the 45° bent  
189 posture and in Table 3 for the 90° bent posture for each of the irradiation geometries.  
190 Organ dose coefficients that showed strong posture variation are depicted in Figs. 3-11<sup>1</sup>.

191 When analyzing ratios of the organ absorbed dose coefficients, it is important to  
192 note that a ratio greater than one (ratio >1) means that the coefficient derived for the  
193 upright posture is less than that based on the bent posture. If the ratio is less than one,  
194 then the opposite holds where the dose for the upright posture is greater than the bent

---

<sup>1</sup> Supplemental electronic data has been provided in Tables 5-40 and Figures 16-25 for sex-specific organ dose coefficients for all organs and neutron energies for AP, PA, LLAT, and RLAT irradiation geometries.

195 posture. The ratios calculated for the AP irradiation geometry show significant  
196 differences between the bent and upright postures, and these differences become more  
197 pronounced with increasing bending angle. The brain receives higher doses in the bent  
198 postures than the upright; it receives as much as 65% for the 45° posture at  $1 \cdot 10^{-9}$  MeV  
199 and 90% more dose for the 90° posture at the 1 MeV neutron energy (Fig 3). There is no  
200 distance-dependence for a parallel beam source in a vacuum; therefore, the fact that the  
201 ratio is greatest at the lower neutron energies suggests that the photon contribution is  
202 higher in the bent geometry. While the brain dose is greater in the bent than in the upright  
203 phantom, all other organs receive a smaller dose for the AP geometry. Most notably, the  
204 thyroid shows the lowest ratio (a lower dose received) (Table 3). The thyroid receives  
205 77% less dose in the half-bent posture and 94% for the full bent posture at the 1 MeV  
206 neutron energy (Table 2). The ratio decreases as a function of energy from  $1 \cdot 10^{-9}$  to 1  
207 MeV and increases as a function of energy from 1 to 20 MeV, meaning that the dose to  
208 the phantom in the 45° posture (Table 2) approaches the dose to the upright phantom<sup>2</sup>.  
209 For the 90° posture, the doses to the abdominal organs (liver, bladder, small intestine,  
210 pancreas, kidneys, gall bladder, adrenals, stomach) are much higher for the upright  
211 phantom than for the bent, and the thoracic organs (extrathoracic region, lungs, breast)  
212 are better represented by the upright phantom than other organs (Table 3).

213 For the PA irradiation geometry, the urinary bladder, testes, and prostate become  
214 more susceptible to increased exposure in a bent posture, where the absorbed doses to all  
215 other organs are less than in the upright phantom (Fig 4, Fig 9-10). Clearly, absorbed  
216 organ dose is dependent on posture; the testes and prostate receive more dose in the full-  
217 bent posture, as these organs are more exposed to the radiation source in the male  
218 phantom with increasing bending angle. The doses to the urinary bladder are slightly  
219 lower in the half-bent posture than in the upright for the  $1 \cdot 10^{-9}$  to 0.5 MeV energy range  
220 and very slightly larger for energies 0.7 to 20 MeV. The dose to the urinary bladder is  
221 lower than in the upright posture by as much as 42% at 0.1 MeV, but only slightly lower  
222 for energies ranging from 2 MeV to 20 MeV in the full-bent posture. The testes show  
223 ratios greater than 1 when compared to the upright male phantom by factors of 2.27 and

---

<sup>2</sup> See supplemental electronic data: Tables 27-28 for organ absorbed dose for thyroid and Figure 16 for ratio plot.

224 4.01 in the 45° and 90° postures, respectively, at 1 MeV. The prostate receives doses that  
225 are higher than those to upright male posture by a factor of 3.03 in the half-bent posture  
226 at 1 MeV and a factor of 2.02 in the full-bent posture at 1.2 MeV. The dose ratios in  
227 Table 2 and Table 3 do not reflect the numbers mentioned above because the tables use  
228 sex-averaged doses, rather than sex-specific doses. Fig 9 and 10 depict the gonad and  
229 sex-specific organ doses, respectively. In the 90° posture, the doses become more  
230 pronounced for the gonads, urinary bladder, bone surface, and uterus/prostate.

231 For both of the lateral geometries (LLAT and RLAT), the organs located in the  
232 torso of the phantom receive more dose than they would have in the upright posture, due  
233 to the lateral geometries having the arms angled out from the body. However, there is  
234 minimal difference in organ doses between the two bent postures, as summarized in  
235 Tables 2 and 3. For the sex-averaged dose ratios, both the breast and thymus receive  
236 lower doses in the full-bent posture than the upright posture for energies 0.05 to 20 MeV,  
237 while all other organs receive doses equal to or greater than the doses to the upright  
238 phantom. For the male phantom, the testes receive lower doses when bent compared to  
239 upright for energies 0.2 to 20 MeV for both of the lateral geometries: as much as 48%  
240 lower for the half-bent posture at 1 MeV (Table 2) and 62% lower for the full bent  
241 posture at 1.2 MeV for both LLAT and RLAT (Table 3)<sup>3</sup>. For both LLAT and RLAT, the  
242 ratios are greater than 1 for the doses for the testes and thymus for lower energies, and the  
243 colon, lungs, stomach, urinary bladder, liver, esophagus, skin, adrenals, small intestine,  
244 kidneys, muscle, uterus/prostate, gall bladder, and heart for all energies, with the  
245 exception of the skin at 20 MeV. For the LLAT geometry, the doses to the spleen and  
246 pancreas in the bent postures are greater than in the upright phantom by factors up to  
247 three. The doses to these organs are greater than the doses for the RLAT geometry  
248 because the pancreas and spleen are located on the left side of the body. The doses differ  
249 from those to the upright phantom so drastically due to the extended arms in the bent  
250 postures, as stated above. Similarly, the liver (Fig 8) receives a higher dose in the RLAT  
251 geometry than the LLAT because it is located in the right side of the body. Overall, there

---

<sup>3</sup> See supplemental electronic data: Table 11 for organ absorbed dose for testes and Figure 24 for ratio plot.

252 is little variation between the two bent postures because the organs observe the same  
253 neutron fluence from the source.

#### 254 Dose to the eye

255 The dose to the eye does not contribute to the effective dose as defined in ICRP  
256 Publication 103. However, the dose to the lens of the eye is an important consideration  
257 among medical and other radiation workers (e.g., Barnard et al. 2016). The dose depends  
258 very strongly on phantom posture in both AP and PA geometries and is generally lower  
259 in the bent phantoms than in the upright and trends towards the dose to the upright  
260 phantom with increasing energy, with the exception of the full-bent phantom in the PA  
261 geometry (Fig 11). There is little variation in the dose to the eye at either LLAT or RLAT  
262 irradiation geometries for all postures; the doses are very near those of the upright  
263 phantom.

#### 264 Contribution of secondary particles

265 For both the active marrow and endosteum doses, photons contribute significantly to the  
266 organ absorbed dose and effective dose coefficients, even more so than the neutrons, for  
267 energies  $1 \cdot 10^{-9}$  to 0.1 MeV for all irradiation geometries. From approximately 0.5 to 20  
268 MeV, the neutrons dominate the dose coefficients. This is true for all phantom postures.  
269 These trends correlate with the plot of the neutron weighting factors, as neutrons have a  
270 larger impact in the mid-energy range and a smaller impact for low and high energies,  
271 where photons increasingly contribute. The neutron and photon contributions to the  
272 absorbed organ dose coefficients for the upright and bent postures can be seen in Fig 12  
273 for the active marrow and Fig 13 for the endosteum for the AP irradiation geometry.

#### 274 Effective dose coefficient

275 The effective dose coefficient was calculated with Eqs. 1 and 2 using gender-averaged  
276 organ equivalent dose coefficients and tissue and radiation weighting factors of ICRP  
277 Publication 103. The effective dose coefficient was expressed as  $\text{pSv}\cdot\text{cm}^2$  for each of the  
278 five irradiation geometries for each posture (upright, half bent, and full bent), and can be  
279 found in Table 4.

280           The most recognizable difference in effective dose coefficients between the  
281 upright and bent postures can be found in the full-bent phantom for the AP geometry,  
282 with the largest discrepancy measuring at 82% lower than that in the upright phantom, at  
283 10 – 50 keV. The phantom in the 90° posture shows effective dose ratios (compared to  
284 upright) of less than 1 for all energies in the AP geometry (Fig 14). The coefficients for  
285 the half-bent phantom are comparable to the upright phantom for energies above 2 MeV.  
286 However, the coefficients are lower than in the upright phantom by as much as 43% for  
287 energies 2 MeV or less.

288           The results for the effective dose coefficients for the PA irradiation geometry  
289 behave similarly to those of the AP geometry (Fig 14). The relative difference to the  
290 upright phantom peaks at 82% for the full-bent phantom, and the 45° bent phantom shows  
291 lower effective dose coefficients when compared to the upright phantom, more so than  
292 for the AP source geometry, over all energies, peaking at 52% lower than the upright  
293 phantom.

294           Contrary to the results for the AP and PA irradiation geometries, the LLAT and  
295 RLAT effective dose coefficient ratios tend to have a position-independent impact, but  
296 still vary as a function of source neutron energy (Fig 15). The relative difference to the  
297 upright phantom ranges from 44% to 15% for the half-bent phantom and 46% to 15% for  
298 the full-bent posture for the LLAT geometry and from 40% to 0% for the both the bent  
299 phantom postures for the RLAT source geometry.

300           PIMAL upright phantom, whose values are found in Table 4, represent the  
301 effective dose values from ICRP Publication 116 well for the AP and PA irradiation  
302 geometries (ICRP 2010). The value for the effective dose in the AP geometry at  $1 \cdot 10^{-5}$   
303 MeV is 0.32% greater than that in the ICRP document, and the greatest difference occurs  
304 at 20 MeV, which is 29% less than the dose published by the ICRP. For the PA geometry,  
305 the effective dose from this work is 1.74% and 46.74% greater than the ICRP's value at 4  
306 MeV and 0.2 MeV, respectively. The LLAT geometry shows relative differences ranging

307 from 0.58% greater at 0.07 MeV to 37.18% less at 20 MeV. The RLAT geometry values  
308 range from 0.81% greater at 0.005 MeV to 37.90% less at 20 MeV.<sup>4</sup>

309

## 310 **Conclusion**

311 Organ and effective dose coefficients were simulated for phantoms in half- and full-bent  
312 articulated positions and compared to the traditional upright phantom. Monoenergetic  
313 neutron irradiation fields were simulated for AP, PA, LLAT, and RLAT source  
314 geometries for energies ranging from  $1 \cdot 10^{-9}$  MeV to 20 MeV. Because the effective  
315 dose coefficients for the articulated phantoms were lower than those of the upright  
316 phantom for all energies for both the AP and PA geometries, using the upright phantom  
317 would provide a conservative approach to determining effective dose. This may result in  
318 a higher-than-actual assigned dose to the receptor, which may be impactful in certain  
319 dose estimation or dose reconstruction scenarios. Both the organ absorbed dose and  
320 effective dose coefficients for the articulated phantoms were generally higher than the  
321 coefficients for the upright phantom in the LLAT and RLAT source geometries for both  
322 bent phantom postures.

323 Effective dose is a robust quantity, but consideration must be given to organs at  
324 risk for a receptor in an articulated position. The absorbed dose coefficients of the brain  
325 for the AP irradiation source geometry and the testes and prostate for the PA irradiation  
326 source geometry for both bent phantom postures are significantly higher than those of the  
327 upright phantom. This warrants that the posture of the receptor, as well as the location  
328 and energies of source radiation fields and source geometries, must be considered when  
329 calculating absorbed dose, in order to obtain an accurate understanding of the dose  
330 received by the organs. It is important to take realistic working postures into  
331 consideration to determine accurate results when performing dose estimations, especially

---

<sup>4</sup> An expanded library of graphs of the ratios comparing the postures to the upright PIMAL phantom has been provided as electronic supplemental material as Figs 16-25 for each sex-averaged organs and the AP, PA, LLAT, and RLAT sources.

332 noting where organ doses for receptors in articulated positions may be under- or over-  
333 estimated in the absence of employing an articulated phantom for dose estimation.

334

335 **Acknowledgements** The authors would like to thank Dr. Keith Eckerman and Dr. Ken  
336 Veinot for their invaluable feedback on this work. This work was supported in part by the  
337 U.S. Department of Energy, Office of Science, Office of Workforce Development for  
338 Teachers and Scientists (WDTS) under the Science Undergraduate Laboratory Internship  
339 program and by the United States Nuclear Regulatory Commission under Contract No.  
340 NRCHQ6017D0003.

341

342 **References**

- 343 Akkurt H, Eckerman KF. (2007) Development of PIMAL: Mathematical Phantom with  
344 Moving Arms and Legs, ORNL/TM-2007/14. Oak Ridge National Laboratory,  
345 Oak Ridge
- 346 Akkurt H, Bekar K, Eckerman KF (2009) Assessment of Organ Doses for a Glovebox  
347 Worker Using Realistic Postures with PIMAL and VOXMAT. *Trans Am Nuc Soc*  
348 101:671-3
- 349 Alves M, Santos W, Lee C, Bolch W, Hunt J, Júnior AC (2016) Conversion coefficients  
350 for proton beams using standing and sitting male hybrid computational phantom  
351 calculated in idealized irradiation geometries. *Radiat Prot Dosim* 175(1), 75-86
- 352 Barnard SG, Ainsbury EA, Quinlan RA, Bouffler SD (2016) Radiation protection of the  
353 eye lens in medical workers—basis and impact of the ICRP recommendations.  
354 *Brit J Radiol* 89(1060), 20151034
- 355 Bellamy MB, Hiller MM, Dewji SA, Veinot KG, Leggett RW, Eckerman KF, Easterly C,  
356 Hertel NE (2016) Comparison of monoenergetic photon organ dose rate  
357 coefficients for stylized and voxel phantoms submerged in air. *Radiat Prot Dosim*  
358 172(4), 367-374
- 359 Dewji SA, Bellamy MB, Hertel NE, Leggett RW, Sherbini S, Saba MS, Eckerman KF  
360 (2015) Estimated dose rates to members of the public from external exposure to  
361 patients with <sup>131</sup>I thyroid treatment. *Med Phys* 42(4), 1851-1857
- 362 Dewji SA, Hiller MM (2016) PIMAL: Phantom wIth Moving Arms and Legs Version  
363 4.1.0. US Nuclear Regulatory Commission, Rockville, NUREG/CR-7131
- 364 Dewji SA, Reed KL, Hiller MM (2017) Comparison of Organ Doses for PIMAL Stylized  
365 Phantoms in Upright and Bent Positions for Standard Irradiation Geometries.  
366 *Radiat Environ Biophys* 56(3):277-91



367 Han EY, Ha W.-H., Jin Y-W, Bolch WE, Lee C (2014) Effective dose conversion  
368 coefficients for health care provider exposed to pediatric and adult victims in  
369 radiological dispersal device incident. *J Radiol Prot* 35(1): 37-45

370 Hiller M, Dewji SA (2017) Comparison of monoenergetic photon organ dose rate  
371 coefficients for the female stylized and voxel phantoms submerged in air. *Radiat*  
372 *Prot Dosim* 175(3):336-43

373 International Commission on Radiological Protection (1996) ICRP Publication 74:  
374 Conversion coefficients for use in radiological protection against external  
375 radiation. In: *Annals of the ICRP* 26 (3-4)

376 International Commission on Radiological Protection (2002) ICRP Publication 89: Basic  
377 anatomical and physiological data for use in radiological protection: reference  
378 values. In: *Annals of the ICRP* 32

379 International Commission on Radiological Protection (2007) ICRP Publication 103: The  
380 2007 Recommendations of the International Commission on Radiological  
381 Protection. In: *Annals of the ICRP* 37

382 International Commission on Radiological Protection (2009) ICRP Publication 110:  
383 Adult reference computational phantoms. In: *Annals of the ICRP* 39

384 International Commission on Radiological Protection (2010) ICRP Publication 116:  
385 Conversion coefficients for radiological protection quantities for external  
386 radiation exposures. In: *Annals of the ICRP* 40

387 Pelowitz DB, Fallgren AJ, McMath GE (2014) MCNP6 User's Manual, Code Version  
388 6.1.1 beta. Los Alamos National Laboratory, Los Alamos

389 Vazquez JA, Caracappa PF, Xu XG (2014) Development of posture- specific  
390 computational phantoms using motion capture technology and application to  
391 radiation dose-reconstruction for the 1999 Tokai-Mura nuclear criticality  
392 accident. *Phys Med Biol* 59(18):5277-5286

393 Xu XG (2014) An exponential growth of computational phantom research in radiation  
394 protection, imaging, and radiotherapy: a review of the fifty-year history. Phys  
395 Med Biol 59 (18):R233-R302

396

397

398 **List of Tables**

399 **Table 1** ICRP Publication 103 tissue weighting factors (International Commission on  
400 Radiological Protection 2007).

401 **Table 2** Ratios of sex-averaged organ absorbed dose coefficients (45° bent/upright) for  
402 AP, PA, LLAT and RLAT irradiation geometries for selected neutron energies from 0.01  
403 MeV to 20 MeV. AP – antero – posterior; PA – postero – anterior; LLAT – left lateral;  
404 RLAT – right lateral

405 **Table 3** Ratios of sex-averaged organ absorbed dose coefficients (90° bent/upright) for  
406 AP, PA, LLAT, and RLAT irradiation geometries for selected neutron energies from 0.01  
407 MeV to 20 MeV. AP – antero – posterior; PA – postero – anterior; LLAT – left lateral;  
408 RLAT – right lateral

409

410 **Table 4** Effective dose coefficients (pSv cm<sup>2</sup>) for AP, PA, LLAT, and RLAT irradiation  
411 geometries for upright, 45°, and 90° bent postures for neutron energies of  $1 \cdot 10^{-9}$  to 20  
412 MeV. AP – antero – posterior; PA – postero – anterior; LLAT – left lateral; RLAT – right  
413 lateral

414 **Table 2** Ratios of sex-averaged organ absorbed dose coefficients (45° bent/upright) for AP, PA,  
 415 LLAT and RLAT irradiation geometries for selected neutron energies from 0.01 MeV to 20 MeV.  
 416 AP – antero – posterior; PA – postero – anterior; LLAT – left lateral; RLAT – right lateral

Energy	45° bent/upright								
	AP								
Organs/tissues	0.01 MeV	0.05 MeV	0.1 MeV	0.5 MeV	1 MeV	5 MeV	10 MeV	15 MeV	20 MeV
Gonads	0.72	0.66	0.72	0.71	0.73	0.89	0.95	1.03	1.12
Bone Marrow	0.82	0.82	0.83	0.85	0.88	0.91	0.92	0.91	0.96
Colon	0.61	0.60	0.59	0.55	0.54	0.75	0.84	0.92	1.04
Lungs	0.71	0.71	0.68	0.62	0.62	0.83	0.90	0.97	1.07
Stomach	0.61	0.61	0.60	0.58	0.60	0.83	0.91	0.99	1.11
Urinary bladder	0.69	0.67	0.64	0.63	0.65	0.87	0.94	1.02	1.13
Breast	0.81	0.83	0.85	0.93	0.95	1.04	1.07	1.12	1.16
Liver	0.58	0.58	0.57	0.56	0.58	0.79	0.87	0.94	1.05
Esophagus	0.73	0.78	0.71	0.72	0.69	0.74	0.82	0.87	0.97
Thyroid	0.83	0.63	0.48	0.24	0.23	0.45	0.56	0.63	0.74
Skin	0.76	0.87	0.92	0.97	0.98	0.98	1.02	1.09	1.16
Bone Surface	0.85	0.85	0.85	0.88	0.91	0.95	0.96	0.95	0.98
Adrenals	0.58	0.66	0.60	0.66	0.64	0.64	0.72	0.75	0.84
Brain	1.49	1.52	1.55	1.59	1.59	1.26	1.23	1.24	1.27
Extrathoracic airways	0.87	0.86	0.75	0.40	0.35	0.51	0.62	0.69	0.78
Small intestine	0.62	0.61	0.61	0.56	0.55	0.73	0.82	0.89	1.01
Kidneys	0.57	0.57	0.57	0.57	0.55	0.56	0.66	0.72	0.83
Muscle	0.67	0.69	0.70	0.75	0.78	0.86	0.91	0.95	1.04
Pancreas	0.59	0.59	0.59	0.55	0.53	0.67	0.76	0.84	0.95
Spleen	0.51	0.51	0.54	0.51	0.50	0.62	0.72	0.78	0.90
Thymus	0.80	0.75	0.70	0.70	0.73	0.95	1.00	1.07	1.15
Uterus/Prostate	0.63	0.66	0.67	0.56	0.55	0.75	0.84	0.90	1.01
Eyes	0.88	0.81	0.79	0.84	0.86	0.99	1.04	1.10	1.14
Gall bladder	0.60	0.62	0.67	0.56	0.56	0.77	0.87	0.93	1.06
Heart	0.68	0.66	0.66	0.62	0.63	0.83	0.91	0.98	1.08
Oral mucosa	0.88	0.85	0.80	0.68	0.68	0.85	0.91	0.96	1.03
Salivary glands	0.90	0.85	0.84	0.67	0.66	0.84	0.90	0.95	1.03

417

Energy	45° bent/upright								
	PA								
Organs/tissues	0.01 MeV	0.05 MeV	0.1 MeV	0.5 MeV	1 MeV	5 MeV	10 MeV	15 MeV	20 MeV
Gonads	0.92	1.00	1.03	1.15	1.23	1.03	1.03	1.07	1.14
Bone Marrow	0.72	0.71	0.71	0.72	0.75	0.89	0.92	0.92	0.97
Colon	0.67	0.68	0.69	0.68	0.68	0.72	0.79	0.85	0.96
Lungs	0.61	0.60	0.58	0.55	0.57	0.76	0.85	0.92	1.02
Stomach	0.61	0.59	0.59	0.55	0.56	0.58	0.68	0.73	0.85
Urinary bladder	0.96	0.92	0.92	1.03	1.15	1.12	1.10	1.12	1.21
Breast	0.78	0.74	0.76	0.64	0.73	0.40	0.48	0.52	0.59
Liver	0.55	0.55	0.55	0.52	0.53	0.68	0.76	0.81	0.92
Esophagus	0.60	0.61	0.60	0.54	0.53	0.72	0.80	0.87	0.96
Thyroid	0.59	0.58	0.56	0.38	0.32	0.47	0.60	0.68	0.80
Skin	0.65	0.75	0.78	0.83	0.85	0.87	0.92	1.00	1.08
Bone Surface	0.78	0.76	0.76	0.80	0.82	0.94	0.95	0.96	1.00
Adrenals	0.61	0.60	0.63	0.56	0.58	0.83	0.91	0.96	1.09
Brain	0.69	0.67	0.66	0.66	0.67	0.87	0.95	1.02	1.11
Extrathoracic airways	0.58	0.57	0.51	0.41	0.40	0.62	0.73	0.83	0.93
Small intestine	0.62	0.62	0.62	0.58	0.56	0.66	0.76	0.82	0.93
Kidneys	0.61	0.61	0.58	0.61	0.64	0.89	0.95	1.03	1.13
Muscle	0.65	0.66	0.67	0.70	0.72	0.82	0.88	0.92	1.00
Pancreas	0.59	0.60	0.58	0.55	0.53	0.67	0.76	0.82	0.93
Spleen	0.55	0.54	0.55	0.52	0.54	0.8	0.88	0.96	1.07
Thymus	0.75	0.69	0.72	0.66	0.72	0.57	0.64	0.66	0.78
Uterus/Prostate	0.93	0.96	1.12	1.55	1.76	1.25	1.19	1.19	1.24
Eyes	0.77	0.81	0.73	0.73	0.74	0.58	0.67	0.72	0.85
Gall bladder	0.66	0.60	0.63	0.61	0.59	0.59	0.71	0.74	0.83
Heart	0.64	0.64	0.63	0.58	0.57	0.57	0.66	0.72	0.83
Oral mucosa	0.67	0.67	0.66	0.55	0.51	0.56	0.66	0.73	0.82
Salivary glands	0.65	0.66	0.65	0.52	0.45	0.53	0.64	0.70	0.80

418

Energy	45° bent/upright								
	LLAT								
Organs/tissues	0.01 MeV	0.05 MeV	0.1 MeV	0.5 MeV	1 MeV	5 MeV	10 MeV	15 MeV	20 MeV
Gonads	1.76	1.61	1.45	1.01	0.95	1.08	1.14	1.18	1.24
Bone Marrow	1.21	1.20	1.19	1.15	1.14	1.10	1.10	1.07	1.09
Colon	1.79	1.79	1.81	2.02	2.12	1.79	1.64	1.58	1.62

Lungs	1.70	1.69	1.73	2.10	2.19	1.71	1.58	1.55	1.57
Stomach	1.88	1.92	1.91	1.82	1.79	1.45	1.38	1.38	1.40
Urinary bladder	1.55	1.56	1.63	1.53	1.35	1.21	1.21	1.23	1.28
Breast	1.47	1.31	1.21	1.10	1.07	1.08	1.09	1.11	1.13
Liver	1.74	1.69	1.70	1.67	1.61	1.47	1.43	1.40	1.46
Esophagus	1.55	1.50	1.58	1.72	1.70	1.85	1.69	1.63	1.66
Thyroid	1.08	1.07	1.08	1.02	1.00	1.01	1.05	1.11	1.15
Skin	1.38	1.31	1.28	1.20	1.18	1.08	1.10	1.13	1.16
Bone Surface	1.10	1.10	1.09	1.07	1.07	1.09	1.09	1.07	1.09
Adrenals	1.72	1.63	1.79	1.57	1.63	1.26	1.22	1.22	1.25
Brain	1.13	1.11	1.09	1.04	1.02	1.03	1.06	1.10	1.16
Extrathoracic airways	1.09	1.15	1.08	1.02	1.03	1.03	1.06	1.11	1.17
Small intestine	1.80	1.78	1.79	1.86	1.92	1.72	1.60	1.55	1.59
Kidneys	1.69	1.70	1.66	1.41	1.32	1.14	1.14	1.15	1.20
Muscle	1.66	1.65	1.65	1.59	1.54	1.25	1.23	1.23	1.26
Pancreas	1.94	1.97	2.11	2.52	2.70	2.20	1.92	1.82	1.83
Spleen	2.16	2.11	2.16	2.74	2.84	1.86	1.66	1.61	1.60
Thymus	1.42	1.55	1.42	1.30	1.11	0.95	0.97	0.99	1.04
Uterus/Prostate	1.48	1.55	1.55	1.59	1.47	1.50	1.42	1.39	1.44
Eyes	0.97	1.01	0.99	1.02	1.02	1.04	1.07	1.12	1.17
Gall bladder	1.53	1.79	1.74	1.65	1.75	1.61	1.51	1.44	1.53
Heart	1.75	1.71	1.74	1.77	1.77	1.50	1.44	1.42	1.46
Oral mucosa	1.09	1.07	1.08	1.04	1.03	1.03	1.06	1.10	1.15
Salivary glands	1.08	1.07	1.06	1.05	1.02	1.04	1.06	1.09	1.15

419

Organs/tissues	Energy 45° bent/upright								
	RLAT								
	0.01 MeV	0.05 MeV	0.1 MeV	0.5 MeV	1 MeV	5 MeV	10 MeV	15 MeV	20 MeV
Gonads	1.59	1.49	1.47	1.10	1.02	1.07	1.15	1.19	1.27
Bone Marrow	1.21	1.20	1.19	1.15	1.14	1.10	1.09	1.07	1.09
Colon	1.78	1.80	1.83	1.92	1.98	1.67	1.56	1.52	1.57
Lungs	1.68	1.69	1.74	2.11	2.19	1.72	1.59	1.56	1.57
Stomach	1.78	1.75	1.75	1.71	1.68	1.46	1.41	1.39	1.43
Urinary bladder	1.54	1.52	1.47	1.49	1.36	1.21	1.21	1.22	1.26
Breast	1.47	1.29	1.21	1.09	1.07	1.08	1.09	1.11	1.13
Liver	2.07	2.16	2.27	2.75	2.77	1.70	1.54	1.50	1.49
Esophagus	1.53	1.54	1.56	1.61	1.71	1.82	1.67	1.60	1.63
Thyroid	1.13	1.08	1.13	1.01	1.01	1.01	1.05	1.10	1.15
Skin	1.38	1.31	1.27	1.20	1.18	1.08	1.10	1.13	1.16
Bone Surface	1.10	1.10	1.09	1.07	1.07	1.09	1.09	1.07	1.09
Adrenals	1.70	1.72	1.67	1.53	1.51	1.25	1.21	1.22	1.26
Brain	1.12	1.11	1.09	1.03	1.02	1.03	1.06	1.10	1.16
Extrathoracic airways	1.15	1.13	1.04	1.03	1.03	1.04	1.07	1.11	1.18
Small intestine	1.76	1.78	1.80	1.86	1.90	1.72	1.61	1.56	1.60
Kidneys	1.70	1.71	1.63	1.43	1.33	1.14	1.14	1.15	1.20
Muscle	1.62	1.62	1.61	1.53	1.48	1.23	1.21	1.22	1.26
Pancreas	1.76	1.74	1.75	1.73	1.75	1.93	1.78	1.70	1.75
Spleen	1.57	1.71	1.63	1.63	1.60	1.59	1.52	1.49	1.55
Thymus	1.35	1.36	1.43	1.20	1.11	0.96	0.98	1.01	1.05
Uterus/Prostate	1.52	1.48	1.48	1.46	1.44	1.48	1.43	1.39	1.45
Eyes	1.06	1.04	1.04	1.02	1.02	1.04	1.07	1.13	1.18
Gall bladder	1.80	1.80	1.84	1.75	1.86	1.67	1.58	1.46	1.49
Heart	1.71	1.69	1.75	1.87	1.87	1.59	1.49	1.47	1.50
Oral mucosa	1.10	1.10	1.08	1.04	1.03	1.03	1.06	1.10	1.15
Salivary glands	1.09	1.10	1.04	1.05	1.04	1.03	1.06	1.09	1.15

420  
421

422 **Table 3** Ratios of sex-averaged organ absorbed dose coefficients (90° bent/upright) for AP, PA,  
 423 LLAT, and RLAT irradiation geometries for selected neutron energies from 0.01 MeV to 20  
 424 MeV. AP – antero – posterior; PA – postero – anterior; LLAT – left lateral; RLAT – right lateral

Energy	90° bent/upright								
	AP								
Organs/tissues	0.01 MeV	0.05 MeV	0.1 MeV	0.5 MeV	1 MeV	5 MeV	10 MeV	15 MeV	20 MeV
Gonads	0.23	0.19	0.15	0.09	0.07	0.05	0.06	0.07	0.08
Bone Marrow	0.50	0.50	0.50	0.52	0.55	0.60	0.61	0.61	0.63
Colon	0.08	0.08	0.07	0.05	0.04	0.03	0.06	0.08	0.11
Lungs	0.25	0.24	0.23	0.21	0.22	0.41	0.48	0.52	0.58
Stomach	0.08	0.07	0.07	0.04	0.04	0.09	0.15	0.19	0.25
Urinary bladder	0.14	0.13	0.11	0.05	0.05	0.03	0.04	0.04	0.05
Breast	0.30	0.33	0.36	0.48	0.51	0.76	0.83	0.90	0.96
Liver	0.09	0.08	0.08	0.05	0.04	0.12	0.18	0.23	0.28
Esophagus	0.24	0.23	0.23	0.20	0.18	0.18	0.24	0.27	0.31
Thyroid	0.35	0.27	0.20	0.07	0.06	0.16	0.25	0.31	0.37
Skin	0.29	0.29	0.29	0.31	0.33	0.40	0.43	0.46	0.50
Bone Surface	0.61	0.61	0.61	0.64	0.68	0.75	0.75	0.76	0.78
Adrenals	0.12	0.12	0.12	0.10	0.11	0.11	0.14	0.17	0.20
Brain	1.34	1.48	1.61	1.86	1.90	1.34	1.24	1.19	1.15
Extrathoracic airways	0.44	0.42	0.37	0.17	0.16	0.33	0.42	0.47	0.53
Small intestine	0.08	0.08	0.07	0.04	0.04	0.03	0.05	0.07	0.10
Kidneys	0.10	0.10	0.09	0.08	0.08	0.10	0.15	0.18	0.22
Muscle	0.19	0.18	0.18	0.17	0.18	0.21	0.24	0.26	0.29
Pancreas	0.09	0.08	0.08	0.06	0.06	0.09	0.14	0.17	0.21
Spleen	0.10	0.09	0.09	0.08	0.07	0.23	0.32	0.35	0.42
Thymus	0.16	0.14	0.12	0.06	0.05	0.10	0.16	0.21	0.25
Uterus/Prostate	0.13	0.13	0.12	0.07	0.06	0.02	0.03	0.04	0.05
Eyes	0.36	0.23	0.18	0.19	0.22	0.61	0.69	0.75	0.80
Gall bladder	0.07	0.07	0.07	0.05	0.04	0.04	0.07	0.10	0.13
Heart	0.13	0.13	0.12	0.07	0.07	0.10	0.14	0.18	0.22
Oral mucosa	0.35	0.34	0.30	0.17	0.18	0.44	0.55	0.61	0.67
Salivary glands	0.36	0.36	0.33	0.19	0.21	0.43	0.54	0.59	0.66

425

Energy	90° bent/upright								
	PA								
Organs/tissues	0.01 MeV	0.05 MeV	0.1 MeV	0.5 MeV	1 MeV	5 MeV	10 MeV	15 MeV	20 MeV
Gonads	0.72	0.80	0.91	1.43	1.60	0.94	0.88	0.86	0.85
Bone Marrow	0.38	0.35	0.33	0.29	0.28	0.42	0.45	0.48	0.50
Colon	0.20	0.20	0.21	0.21	0.21	0.27	0.34	0.38	0.45
Lungs	0.11	0.10	0.09	0.04	0.03	0.02	0.04	0.05	0.07
Stomach	0.16	0.15	0.15	0.11	0.12	0.07	0.10	0.13	0.17
Urinary bladder	0.60	0.59	0.58	0.68	0.79	0.95	0.94	0.94	0.97
Breast	0.43	0.41	0.41	0.42	0.46	0.32	0.37	0.36	0.39
Liver	0.11	0.10	0.10	0.06	0.05	0.04	0.07	0.10	0.14
Esophagus	0.06	0.06	0.06	0.04	0.03	0.02	0.04	0.05	0.08
Thyroid	0.07	0.07	0.06	0.03	0.02	0.01	0.02	0.03	0.04
Skin	0.15	0.11	0.10	0.09	0.10	0.17	0.21	0.26	0.30
Bone Surface	0.57	0.55	0.53	0.55	0.57	0.70	0.72	0.73	0.75
Adrenals	0.04	0.04	0.04	0.02	0.01	0.02	0.04	0.07	0.10
Brain	0.04	0.04	0.03	0.01	0.01	0.02	0.02	0.03	0.04
Extrathoracic airways	0.04	0.04	0.04	0.02	0.01	0.01	0.02	0.03	0.03
Small intestine	0.12	0.12	0.12	0.09	0.08	0.16	0.25	0.31	0.38
Kidneys	0.04	0.03	0.03	0.01	0.01	0.03	0.07	0.10	0.15
Muscle	0.16	0.15	0.14	0.11	0.10	0.18	0.23	0.27	0.31
Pancreas	0.08	0.08	0.07	0.05	0.04	0.04	0.09	0.12	0.17
Spleen	0.05	0.05	0.05	0.02	0.02	0.02	0.04	0.07	0.10
Thymus	0.21	0.19	0.19	0.16	0.17	0.08	0.09	0.10	0.12
Uterus/Prostate	0.48	0.51	0.57	0.89	1.05	1.02	0.99	0.99	1.02
Eyes	0.17	0.17	0.17	0.19	0.25	0.11	0.09	0.10	0.10
Gall bladder	0.13	0.13	0.12	0.09	0.09	0.07	0.13	0.17	0.22
Heart	0.15	0.14	0.13	0.10	0.09	0.04	0.06	0.08	0.11
Oral mucosa	0.08	0.08	0.07	0.05	0.05	0.03	0.04	0.05	0.06
Salivary glands	0.07	0.07	0.06	0.04	0.04	0.03	0.03	0.04	0.05

426

Energy	90° bent/upright								
	LLAT								
Organs/tissues	0.01 MeV	0.05 MeV	0.1 MeV	0.5 MeV	1 MeV	5 MeV	10 MeV	15 MeV	20 MeV
Gonads	1.63	1.53	1.48	1.02	0.90	0.95	1.00	1.03	1.04
Bone Marrow	1.21	1.21	1.20	1.16	1.15	1.09	1.08	1.07	1.06
Colon	1.76	1.73	1.75	1.96	2.07	1.76	1.56	1.48	1.41

Lungs	1.50	1.50	1.56	1.94	2.03	1.61	1.45	1.38	1.33
Stomach	1.82	1.83	1.82	1.78	1.77	1.43	1.33	1.27	1.22
Urinary bladder	1.66	1.62	1.64	1.50	1.42	1.23	1.19	1.17	1.13
Breast	1.17	0.88	0.73	0.55	0.53	0.72	0.78	0.81	0.83
Liver	1.66	1.66	1.65	1.62	1.58	1.46	1.38	1.34	1.30
Esophagus	1.37	1.40	1.44	1.55	1.64	1.81	1.61	1.52	1.46
Thyroid	1.05	1.03	1.04	1.01	1.01	1.00	1.00	1.00	0.99
Skin	1.33	1.27	1.24	1.17	1.16	1.04	1.03	1.01	0.99
Bone Surface	1.14	1.14	1.13	1.09	1.08	1.08	1.09	1.08	1.07
Adrenals	1.59	1.47	1.60	1.51	1.48	1.24	1.18	1.14	1.11
Brain	1.02	1.01	1.01	1.01	1.01	1.00	1.00	1.00	1.00
Extrathoracic airways	1.04	1.05	1.05	1.00	1.01	1.00	1.00	1.00	1.00
Small intestine	1.73	1.73	1.73	1.81	1.87	1.69	1.53	1.45	1.39
Kidneys	1.56	1.56	1.56	1.37	1.30	1.11	1.08	1.06	1.04
Muscle	1.57	1.58	1.58	1.54	1.51	1.22	1.17	1.15	1.12
Pancreas	1.86	1.85	1.93	2.38	2.64	2.15	1.84	1.70	1.61
Spleen	1.95	1.97	2.03	2.64	2.79	1.82	1.57	1.46	1.37
Thymus	1.20	1.22	1.21	0.96	0.80	0.56	0.62	0.65	0.66
Uterus/Prostate	1.46	1.46	1.49	1.53	1.45	1.48	1.38	1.34	1.30
Eyes	1.01	1.03	1.02	1.01	1.00	1.01	1.01	1.01	1.01
Gall bladder	1.65	1.77	1.76	1.66	1.63	1.61	1.48	1.43	1.38
Heart	1.53	1.56	1.53	1.60	1.62	1.45	1.35	1.31	1.27
Oral mucosa	1.03	1.03	1.02	1.02	1.01	1.01	1.01	1.01	1.01
Salivary glands	1.02	1.02	1.02	1.02	1.01	1.01	1.01	1.01	1.01

427

Energy	90° bent/upright								
	RLAT								
Organs/tissues	0.01 MeV	0.05 MeV	0.1 MeV	0.5 MeV	1 MeV	5 MeV	10 MeV	15 MeV	20 MeV
Gonads	1.58	1.62	1.55	1.05	0.90	0.95	1.00	1.03	1.03
Bone Marrow	1.21	1.21	1.20	1.16	1.15	1.09	1.08	1.08	1.06
Colon	1.75	1.74	1.76	1.87	1.94	1.65	1.50	1.42	1.36
Lungs	1.51	1.52	1.56	1.95	2.04	1.62	1.46	1.39	1.33
Stomach	1.73	1.72	1.71	1.70	1.64	1.47	1.37	1.32	1.28
Urinary bladder	1.62	1.59	1.58	1.50	1.42	1.22	1.19	1.17	1.13
Breast	1.16	0.88	0.73	0.55	0.53	0.72	0.78	0.81	0.83
Liver	1.95	2.01	2.14	2.67	2.74	1.67	1.48	1.39	1.31
Esophagus	1.34	1.33	1.39	1.55	1.60	1.76	1.58	1.50	1.44
Thyroid	1.00	1.05	1.03	1.01	1.00	1.00	1.00	1.01	1.00
Skin	1.32	1.27	1.24	1.17	1.16	1.04	1.03	1.01	0.99
Bone Surface	1.14	1.14	1.13	1.09	1.08	1.08	1.09	1.08	1.07
Adrenals	1.48	1.57	1.62	1.54	1.48	1.23	1.16	1.14	1.11
Brain	1.02	1.02	1.01	1.01	1.01	1.00	1.00	1.00	1.00
Extrathoracic airways	1.05	1.04	1.04	1.02	1.01	1.00	1.00	1.00	1.00
Small intestine	1.71	1.72	1.72	1.80	1.85	1.70	1.53	1.46	1.39
Kidneys	1.56	1.56	1.53	1.37	1.30	1.11	1.08	1.06	1.04
Muscle	1.54	1.54	1.54	1.49	1.45	1.20	1.16	1.14	1.11
Pancreas	1.60	1.64	1.64	1.64	1.67	1.90	1.71	1.61	1.55
Spleen	1.57	1.57	1.58	1.60	1.52	1.56	1.47	1.40	1.36
Thymus	1.24	1.25	1.20	0.98	0.83	0.57	0.62	0.65	0.66
Uterus/Prostate	1.51	1.50	1.50	1.47	1.44	1.48	1.39	1.34	1.31
Eyes	1.03	1.00	1.04	1.04	1.01	1.01	1.01	1.01	1.01
Gall bladder	1.72	1.66	1.74	1.78	1.77	1.67	1.52	1.43	1.39
Heart	1.54	1.54	1.57	1.69	1.74	1.53	1.41	1.35	1.30
Oral mucosa	1.03	1.03	1.03	1.01	1.01	1.01	1.01	1.01	1.01
Salivary glands	1.03	1.03	1.01	1.01	1.01	1.01	1.01	1.01	1.01

428  
429  
430



432 **Table 4** Effective dose coefficients (pSv cm<sup>2</sup>) for AP, PA, LLAT, and RLAT irradiation  
 433 geometries for upright, 45°, and 90° bent postures for neutron energies of 1 · 10<sup>-9</sup> to 20 MeV. AP  
 434 – antero – posterior; PA – postero – anterior; LLAT – left lateral; RLAT – right lateral

Irradiation Geometry	Neutron Energy (MeV)	Upright (pSv-cm <sup>2</sup> )	Error (%)	45° Bent (pSv-cm <sup>2</sup> )	Error (%)	Relative difference to upright (%)	90° Bent (pSv-cm <sup>2</sup> )	Error (%)	Relative difference to upright (%)
AP	1.0·10 <sup>-9</sup>	3.11	0.12	2.05	0.11	-34.05	0.89	0.23	-71.29
	1.0·10 <sup>-8</sup>	3.61	0.09	2.33	0.11	-35.60	0.97	0.30	-73.07
	2.5·10 <sup>-8</sup>	4.19	0.08	2.67	0.10	-36.29	1.09	0.30	-73.98
	1.0·10 <sup>-7</sup>	5.37	0.07	3.44	0.09	-35.95	1.29	0.27	-76.00
	2.0·10 <sup>-7</sup>	5.97	0.06	3.82	0.08	-35.98	1.39	0.26	-76.63
	5.0·10 <sup>-7</sup>	6.74	0.06	4.31	0.08	-36.04	1.53	0.25	-77.31
	1.0·10 <sup>-6</sup>	7.15	0.06	4.62	0.07	-35.41	1.59	0.25	-77.72
	2.0·10 <sup>-6</sup>	7.45	0.06	4.82	0.07	-35.36	1.64	0.24	-78.02
	5.0·10 <sup>-6</sup>	7.75	0.10	4.98	0.07	-35.77	1.69	0.25	-78.18
	1.0·10 <sup>-5</sup>	7.84	0.05	5.09	0.06	-35.17	1.71	0.24	-78.22
	2.0·10 <sup>-5</sup>	7.88	0.05	5.12	0.07	-35.10	1.72	0.23	-78.18
	5.0·10 <sup>-5</sup>	7.90	0.05	5.14	0.07	-35.00	1.70	0.24	-78.46
	1.0·10 <sup>-4</sup>	7.86	0.05	5.13	0.05	-34.73	1.71	0.23	-78.19
	2.0·10 <sup>-4</sup>	7.82	0.05	5.11	0.07	-34.65	1.70	0.23	-78.31
	5.0·10 <sup>-4</sup>	7.78	0.05	5.07	0.07	-34.84	1.67	0.24	-78.50
	0.001	7.85	0.05	5.04	0.05	-35.85	1.67	0.23	-78.73
	0.002	8.32	0.09	5.05	0.05	-39.29	1.58	0.24	-81.03
	0.005	9.04	0.05	5.35	0.05	-40.78	1.67	0.24	-81.51
	0.01	10.79	0.03	6.12	0.05	-43.27	1.92	0.09	-82.22
	0.02	14.39	0.05	8.21	0.05	-42.94	2.58	0.23	-82.07
	0.03	18.46	0.09	10.53	0.05	-42.96	3.31	0.24	-82.05
	0.05	26.54	0.03	15.36	0.05	-42.13	4.88	0.09	-81.60
	0.07	34.60	0.05	20.24	0.05	-41.52	6.45	0.24	-81.36
	0.1	47.20	0.03	27.88	0.05	-40.92	9.28	0.09	-80.34
	0.15	68.43	0.04	40.16	0.05	-41.32	13.41	0.23	-80.40
	0.2	88.37	0.04	51.99	0.05	-41.17	17.40	0.24	-80.32
	0.3	121.18	0.04	74.11	0.04	-38.84	25.13	0.23	-79.26
0.5	176.69	0.02	116.21	0.04	-34.23	39.26	0.08	-77.78	
0.7	228.81	0.03	153.98	0.03	-32.70	52.23	0.20	-77.17	
0.9	269.08	0.03	184.04	0.03	-31.61	62.54	0.20	-76.76	
1	267.78	0.02	179.17	0.04	-33.09	62.43	0.07	-76.69	
1.2	319.68	0.04	218.55	0.03	-31.64	74.66	0.18	-76.65	
1.5	356.67	0.03	249.51	0.03	-30.04	85.01	0.17	-76.16	
2	392.69	0.02	286.77	0.02	-26.97	98.52	0.14	-74.91	
3	432.58	0.01	335.71	0.02	-22.39	118.40	0.11	-72.63	
4	453.59	0.02	360.55	0.02	-20.51	127.52	0.10	-71.89	
5	447.34	0.01	366.73	0.01	-18.02	136.05	0.03	-69.59	
7	449.18	0.01	380.79	0.01	-15.23	147.65	0.08	-67.13	
8	446.27	0.01	382.82	0.01	-14.22	151.93	0.07	-65.95	
9	444.21	0.01	381.45	0.02	-14.13	151.80	0.07	-65.83	
10	436.43	0.01	375.81	0.02	-13.89	151.14	0.03	-65.37	
12	429.55	0.02	374.57	0.02	-12.80	152.66	0.07	-64.46	
14	419.46	0.02	373.74	0.02	-10.90	157.45	0.08	-62.46	
15	416.91	0.01	374.49	0.02	-10.18	158.65	0.03	-61.95	
16	357.43	0.02	367.35	0.02	2.78	159.69	0.08	-55.32	
18	348.11	0.02	365.38	0.02	4.96	163.67	0.08	-52.98	
20	338.65	0.02	359.32	0.03	6.10	164.08	0.03	-51.55	
PA	1.0·10 <sup>-9</sup>	2.22	0.13	1.41	0.12	-36.79	0.74	0.31	-66.62
	1.0·10 <sup>-8</sup>	2.62	0.16	1.60	0.12	-38.98	0.80	0.41	-69.43
	2.5·10 <sup>-8</sup>	3.04	0.15	1.84	0.11	-39.54	0.88	0.41	-71.08
	1.0·10 <sup>-7</sup>	3.87	0.13	2.40	0.09	-38.13	1.07	0.37	-72.30
	2.0·10 <sup>-7</sup>	4.31	0.12	2.68	0.09	-37.88	1.16	0.35	-73.15
	5.0·10 <sup>-7</sup>	4.92	0.11	3.08	0.08	-37.48	1.30	0.34	-73.59
	1.0·10 <sup>-6</sup>	5.23	0.11	3.28	0.08	-37.26	1.38	0.34	-73.57
	2.0·10 <sup>-6</sup>	5.50	0.11	3.46	0.08	-37.00	1.42	0.33	-74.14
	5.0·10 <sup>-6</sup>	5.77	0.10	3.61	0.08	-37.35	1.48	0.31	-74.38
	1.0·10 <sup>-5</sup>	5.86	0.10	3.68	0.08	-37.10	1.51	0.32	-74.18
2.0·10 <sup>-5</sup>	5.92	0.10	3.75	0.07	-36.65	1.52	0.33	-74.34	

	5.0·10 <sup>-5</sup>	5.96	0.10	3.78	0.07	-36.52	1.52	0.31	-74.49
	1.0·10 <sup>-4</sup>	5.95	0.10	3.78	0.07	-36.45	1.53	0.32	-74.25
	2.0·10 <sup>-4</sup>	5.99	0.10	3.79	0.07	-36.67	1.54	0.31	-74.23
	5.0·10 <sup>-4</sup>	6.01	0.10	3.79	0.07	-36.91	1.51	0.32	-74.85
	0.001	6.21	0.10	3.78	0.07	-39.09	1.51	0.33	-75.71
	0.002	6.61	0.10	3.83	0.07	-42.06	1.52	0.32	-77.01
	0.005	7.29	0.10	4.03	0.07	-44.69	1.59	0.33	-78.15
	0.01	8.92	0.04	4.59	0.07	-48.60	1.81	0.12	-79.67
	0.02	11.68	0.10	6.04	0.07	-48.26	2.35	0.32	-79.91
	0.03	15.02	0.10	7.63	0.07	-49.20	2.95	0.32	-80.37
	0.05	21.04	0.04	10.77	0.07	-48.80	4.13	0.12	-80.38
	0.07	26.82	0.09	13.72	0.07	-48.83	5.29	0.32	-80.27
	0.1	35.66	0.03	18.01	0.07	-49.49	6.87	0.12	-80.73
	0.15	50.69	0.05	24.50	0.07	-51.67	9.35	0.32	-81.56
	0.2	63.24	0.08	30.62	0.06	-51.59	11.53	0.31	-81.77
	0.3	81.27	0.08	41.64	0.06	-48.77	15.77	0.31	-80.59
	0.5	106.37	0.02	62.17	0.05	-41.55	23.51	0.11	-77.89
	0.7	138.38	0.06	82.73	0.05	-40.21	30.45	0.30	-77.99
	0.9	161.16	0.05	98.30	0.04	-39.00	36.05	0.28	-77.63
	1	152.04	0.02	91.30	0.04	-39.95	33.90	0.11	-77.71
	1.2	197.79	0.04	118.83	0.04	-39.92	42.93	0.27	-78.29
	1.5	229.41	0.02	139.96	0.03	-38.99	49.84	0.26	-78.28
	2	262.18	0.03	167.94	0.02	-35.94	59.23	0.23	-77.41
	3	311.02	0.02	211.27	0.02	-32.07	74.04	0.18	-76.20
	4	335.73	0.02	232.79	0.02	-30.66	82.42	0.14	-75.45
	5	346.85	0.01	249.67	0.02	-28.02	88.99	0.05	-74.34
	7	366.33	0.02	273.93	0.02	-25.22	100.86	0.11	-72.47
	8	372.02	0.02	282.16	0.02	-24.15	105.76	0.10	-71.57
	9	371.39	0.02	282.55	0.02	-23.92	106.25	0.10	-71.39
	10	366.67	0.01	280.33	0.02	-23.55	106.19	0.04	-71.04
	12	367.57	0.02	284.63	0.02	-22.56	109.45	0.10	-70.22
	14	368.06	0.02	291.80	0.02	-20.72	114.95	0.09	-68.77
	15	368.76	0.01	294.46	0.02	-20.15	116.85	0.03	-68.31
	16	310.68	0.02	292.47	0.02	-5.86	117.99	0.10	-62.02
	18	309.38	0.02	296.04	0.02	-4.31	122.63	0.10	-60.36
	20	303.69	0.02	293.93	0.03	-3.21	123.56	0.04	-59.31
LLAT	1.0·10 <sup>-9</sup>	0.91	0.23	1.05	0.16	15.07	1.06	0.20	16.82
	1.0·10 <sup>-8</sup>	1.02	0.18	1.22	0.15	19.77	1.22	0.25	19.72
	2.5·10 <sup>-8</sup>	1.19	0.17	1.43	0.14	20.49	1.44	0.23	21.37
	1.0·10 <sup>-7</sup>	1.48	0.14	1.93	0.12	30.18	1.92	0.19	29.99
	2.0·10 <sup>-7</sup>	1.65	0.13	2.17	0.11	31.95	2.17	0.19	31.83
	5.0·10 <sup>-7</sup>	1.86	0.12	2.51	0.10	35.52	2.52	0.17	35.80
	1.0·10 <sup>-6</sup>	1.97	0.12	2.72	0.10	38.14	2.71	0.17	37.85
	2.0·10 <sup>-6</sup>	2.03	0.12	2.87	0.10	41.18	2.88	0.16	41.58
	5.0·10 <sup>-6</sup>	2.14	0.19	3.00	0.09	40.28	3.03	0.16	41.58
	1.0·10 <sup>-5</sup>	2.17	0.11	3.08	0.09	42.27	3.10	0.15	43.11
	2.0·10 <sup>-5</sup>	2.18	0.11	3.12	0.09	43.47	3.13	0.15	43.99
	5.0·10 <sup>-5</sup>	2.19	0.11	3.15	0.09	44.31	3.13	0.15	43.40
	1.0·10 <sup>-4</sup>	2.19	0.11	3.14	0.09	43.71	3.16	0.15	44.66
	2.0·10 <sup>-4</sup>	2.18	0.11	3.13	0.09	43.61	3.17	0.15	45.59
	5.0·10 <sup>-4</sup>	2.18	0.11	3.12	0.09	43.10	3.14	0.15	43.83
	0.001	2.22	0.11	3.09	0.09	39.30	3.12	0.15	40.53
	0.002	2.37	0.18	3.12	0.09	31.78	3.17	0.15	33.73
	0.005	2.61	0.11	3.28	0.09	25.61	3.34	0.15	27.91
	0.01	3.20	0.07	3.76	0.09	17.78	3.80	0.06	18.81
	0.02	4.25	0.11	5.00	0.09	17.49	5.02	0.15	18.03
	0.03	5.55	0.11	6.37	0.09	14.62	6.33	0.15	13.92
	0.05	8.05	0.06	9.14	0.09	13.49	9.01	0.05	11.98
	0.7	10.56	0.10	11.91	0.08	12.81	11.73	0.14	11.07
	0.1	14.60	0.06	16.12	0.08	10.40	15.47	0.05	5.92
	0.15	21.85	0.16	22.90	0.08	4.78	21.51	0.13	-1.55
	0.2	28.76	0.09	29.48	0.07	2.50	27.33	0.13	-4.95
	0.3	39.22	0.08	41.93	0.07	6.89	38.50	0.12	-1.83
	0.5	55.28	0.05	67.36	0.06	21.86	60.81	0.04	10.02
	0.07	74.97	0.06	92.29	0.05	23.10	83.18	0.09	10.95
	0.9	90.08	0.06	111.38	0.05	23.65	100.89	0.08	12.00
	1	88.17	0.04	103.23	0.05	17.09	91.61	0.03	3.91
	1.2	114.15	0.05	136.49	0.04	19.56	123.80	0.07	8.45
	1.5	132.97	0.04	161.08	0.03	21.14	146.96	0.06	10.52

2	155.04	0.03	191.52	0.03	23.53	176.52	0.05	13.86	
3	186.97	0.02	234.87	0.02	25.62	219.43	0.03	17.36	
4	202.52	0.02	256.24	0.02	26.52	241.04	0.03	19.02	
5	218.15	0.01	270.07	0.02	23.80	255.56	0.01	17.15	
7	236.90	0.02	289.96	0.02	22.40	276.56	0.03	16.74	
8	244.02	0.02	296.17	0.02	21.37	283.53	0.03	16.19	
9	244.72	0.02	295.31	0.02	20.67	283.13	0.03	15.70	
10	243.15	0.01	291.99	0.02	20.08	280.14	0.01	15.21	
12	245.36	0.02	293.92	0.02	19.79	282.96	0.03	15.32	
14	251.29	0.02	298.45	0.02	18.77	288.22	0.04	14.70	
15	252.80	0.02	299.87	0.02	18.62	290.05	0.01	14.74	
16	216.12	0.03	297.23	0.02	37.53	287.49	0.04	33.02	
18	219.12	0.03	298.88	0.03	36.40	289.56	0.04	32.15	
20	217.99	0.02	295.66	0.03	35.63	286.85	0.02	31.58	
RLAT	1.0·10 <sup>-9</sup>	0.83	0.23	0.94	0.16	12.25	0.95	0.20	13.40
	1.0·10 <sup>-8</sup>	0.93	0.30	1.08	0.15	16.11	1.09	0.25	17.02
	2.5·10 <sup>-8</sup>	1.07	0.27	1.27	0.14	18.44	1.26	0.23	17.93
	1.0·10 <sup>-7</sup>	1.33	0.24	1.70	0.12	28.07	1.68	0.20	26.72
	2.0·10 <sup>-7</sup>	1.47	0.22	1.91	0.11	29.53	1.90	0.18	28.88
	5.0·10 <sup>-7</sup>	1.64	0.21	2.21	0.10	34.53	2.22	0.17	35.20
	1.0·10 <sup>-6</sup>	1.76	0.20	2.38	0.10	35.70	2.38	0.16	35.22
	2.0·10 <sup>-6</sup>	1.83	0.19	2.50	0.09	36.66	2.51	0.16	37.07
	5.0·10 <sup>-6</sup>	1.88	0.19	2.62	0.09	39.45	2.62	0.16	39.52
	1.0·10 <sup>-5</sup>	1.92	0.19	2.67	0.09	39.16	2.70	0.15	40.80
	2.0·10 <sup>-5</sup>	1.92	0.18	2.70	0.09	40.67	2.68	0.15	39.47
	5.0·10 <sup>-5</sup>	1.95	0.18	2.72	0.09	39.47	2.72	0.15	39.44
	1.0·10 <sup>-4</sup>	1.95	0.18	2.70	0.09	38.79	2.72	0.15	39.68
	2.0·10 <sup>-4</sup>	1.94	0.18	2.71	0.09	39.68	2.72	0.15	40.03
	5.0·10 <sup>-4</sup>	1.93	0.18	2.68	0.09	39.18	2.69	0.15	39.40
	0.001	1.97	0.18	2.68	0.09	35.82	2.71	0.15	37.45
	0.002	2.12	0.18	2.68	0.09	26.65	2.72	0.15	28.67
	0.005	2.35	0.18	2.82	0.09	20.25	2.84	0.15	20.80
	0.01	2.90	0.07	3.23	0.09	11.23	3.25	0.06	11.87
	0.02	3.86	0.18	4.33	0.09	12.10	4.29	0.15	11.03
	0.03	5.05	0.17	5.51	0.09	9.07	5.46	0.15	7.93
	0.05	7.35	0.06	7.97	0.09	8.44	7.80	0.05	6.13
	0.07	9.65	0.17	10.45	0.08	8.25	10.15	0.14	5.11
	0.1	13.46	0.06	14.15	0.08	5.10	13.53	0.05	0.51
	0.15	20.30	0.15	20.35	0.08	0.25	19.03	0.13	-6.25
	0.2	26.89	0.15	26.39	0.07	-1.85	24.22	0.13	-9.93
	0.3	36.57	0.14	37.90	0.07	3.62	34.20	0.12	-6.50
	0.5	51.01	0.04	61.03	0.06	19.65	54.20	0.04	6.25
	0.7	69.05	0.10	82.84	0.05	19.98	73.44	0.09	6.36
	0.9	82.65	0.09	99.97	0.05	20.95	88.68	0.08	7.30
	1	81.64	0.04	93.18	0.05	14.14	81.24	0.03	-0.48
	1.2	105.01	0.08	121.79	0.04	15.98	108.47	0.07	3.30
	1.5	121.56	0.07	142.77	0.03	17.45	128.32	0.06	5.57
	2	141.21	0.05	169.48	0.03	20.02	153.95	0.05	9.02
	3	169.83	0.04	208.88	0.02	22.99	192.90	0.03	13.58
	4	184.08	0.04	228.06	0.02	23.89	212.47	0.03	15.42
	5	199.22	0.01	242.72	0.02	21.84	228.06	0.01	14.48
	7	217.71	0.03	263.61	0.02	21.08	250.25	0.03	14.95
	8	225.39	0.03	270.72	0.02	20.12	257.99	0.03	14.47
	9	226.24	0.03	270.19	0.02	19.42	257.76	0.03	13.93
	10	224.91	0.01	267.95	0.02	19.14	255.76	0.01	13.72
	12	227.77	0.04	270.80	0.02	18.89	259.32	0.03	13.85
	14	234.69	0.04	276.73	0.02	17.91	266.52	0.04	13.56
	15	236.20	0.02	278.95	0.02	18.10	268.86	0.01	13.82
	16	200.40	0.04	277.47	0.02	38.46	267.68	0.04	33.57
	18	204.50	0.05	280.50	0.03	37.16	271.59	0.04	32.81
	20	203.69	0.02	278.46	0.03	36.71	269.45	0.02	32.28

The error columns give the relative statistical error propagated from the uncertainty of the Monte Carlo simulations.  
Relative difference denotes the percent difference of the effective dose coefficient ratio (bent/upright) from a ratio of 1.00.

435  
436  
437

438 **List of Figures**

439

440 **Fig 1** The upright, half-bent (45°), and full-bent (90°) side views taken from the PIMAL  
441 4.1.0 GUI for the stylized phantom.

442

443 **Fig 2** Neutron weighting factor,  $w_R$ , as a function of neutron energy, shown for energies  
444  $1.0 \cdot 10^{-9} - 20$  MeV.

445

446 **Fig 3** Sex-averaged absorbed dose coefficient ratio for brain in AP and PA irradiation  
447 geometries with PIMAL bent at 45° and 90° postures. A horizontal line for a ratio of 1.0  
448 is provided as a visual reference for the reader.

449

450 **Fig 4** Sex-averaged absorbed dose coefficient ratio for urinary bladder in AP and PA  
451 irradiation geometries with PIMAL bent at 45° and 90° postures. A horizontal line for a  
452 ratio of 1.0 is provided as a visual reference for the reader.

453

454 **Fig 5** Sex-averaged absorbed dose coefficient ratio for skin in AP and PA irradiation  
455 geometries with PIMAL bent at 45° and 90° postures. A horizontal line for a ratio of 1.0  
456 is provided as a visual reference for the reader.

457

458 **Fig 6** Sex-averaged absorbed dose coefficient ratio for endosteum and active marrow in  
459 AP and PA irradiation geometries with PIMAL bent at 45° and 90° postures. A horizontal  
460 line for a ratio of 1.0 is provided as a visual reference for the reader.

461

462 **Fig 7** Sex-averaged absorbed dose coefficient ratio for breast in AP and PA irradiation  
463 geometries with PIMAL bent at 45° and 90° postures. A horizontal line for a ratio of 1.0  
464 is provided as a visual reference for the reader.

465

466 **Fig 8** Sex-averaged absorbed dose coefficient ratio for liver in LLAT and RLAT  
467 irradiation geometries with PIMAL bent at 45° and 90° postures.

468

469 **Fig 9** Absorbed dose coefficient ratio for gonads (male: testes; female: ovaries) in AP and  
470 PA irradiation geometries with PIMAL bent at 45° and 90° postures. A horizontal line for  
471 a ratio of 1.0 is provided as a visual reference for the reader.

472

473 **Fig 10** Absorbed dose coefficient ratio for sex-specific organs (male: prostate; female:  
474 uterus) in AP and PA irradiation geometries with PIMAL bent at 45° and 90° postures. A  
475 horizontal line for a ratio of 1.0 is provided as a visual reference for the reader.

476

477 **Fig 11** Sex-averaged absorbed dose coefficient ratio for eyes in AP and PA irradiation  
478 geometries with PIMAL bent at 45° and 90° postures. A horizontal line for a ratio of 1.0  
479 is provided as a visual reference for the reader.

480

481 **Fig 12** Neutron and photon contributions to the absorbed dose coefficients for active  
482 marrow for selected energies in the AP irradiation geometry (upright male phantom).

483

484 **Fig 13** Neutron and photon contributions to the absorbed dose coefficients for endosteum  
485 for selected energies in the AP irradiation geometry (upright male phantom).

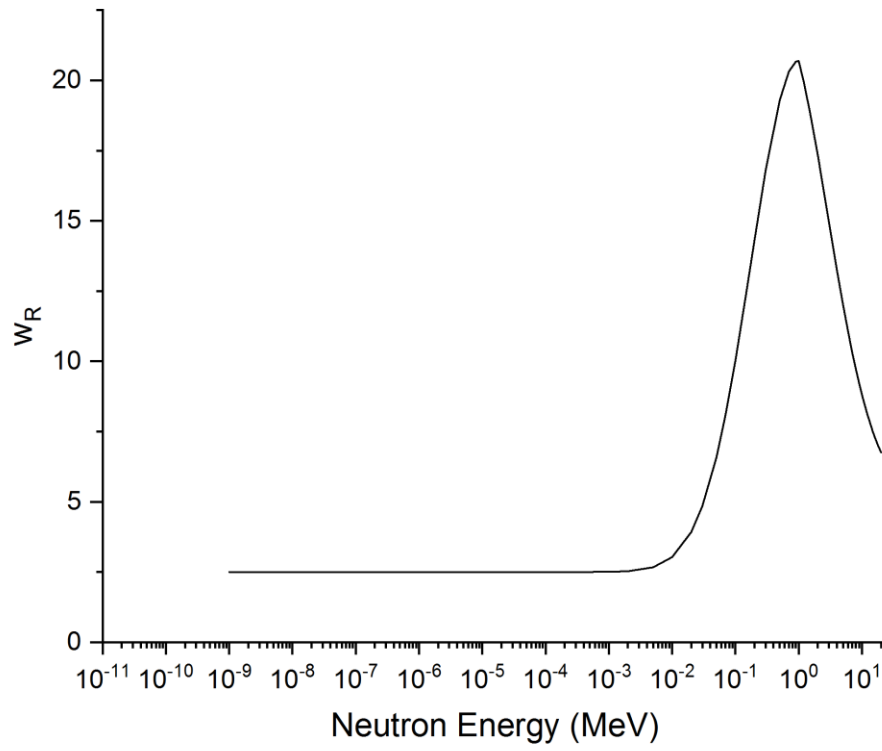
486

487 **Fig 14** Effective dose coefficient ratio in AP and PA irradiation geometries with PIMAL  
488 bent at 45° and 90° postures. A horizontal line for a ratio of 1.0 is provided as a visual  
489 reference for the reader.

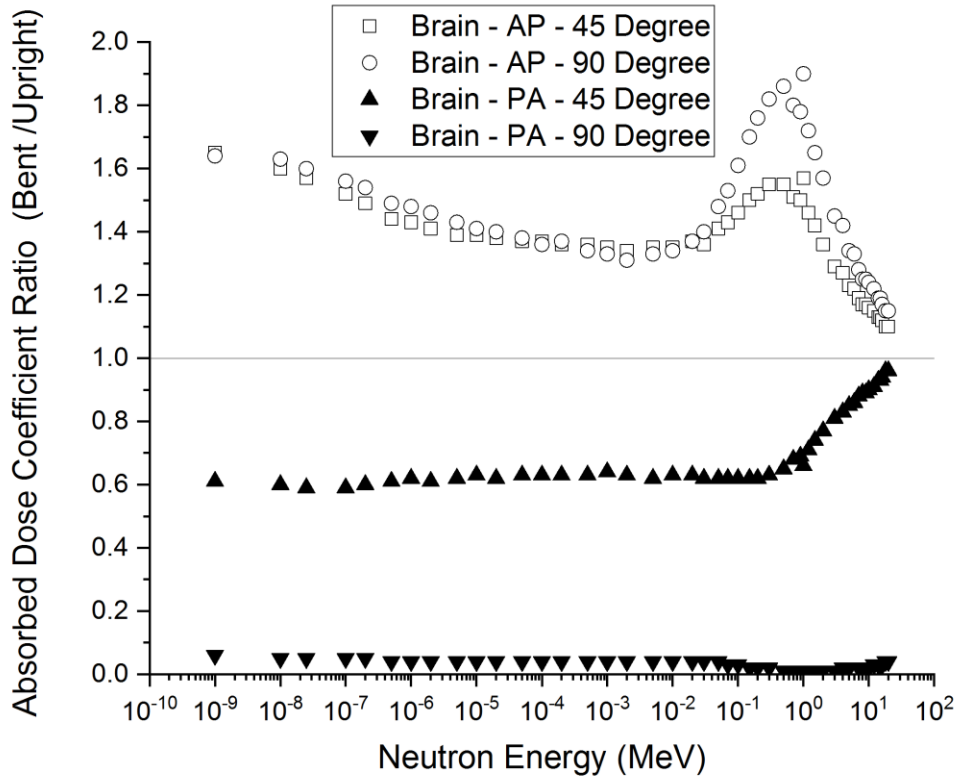
490

491 **Fig 15** Effective dose coefficient ratio in LLAT and RLAT irradiation geometries with  
492 PIMAL bent at 45° and 90° postures. A horizontal line for a ratio of 1.0 is provided as a  
493 visual reference for the reader.

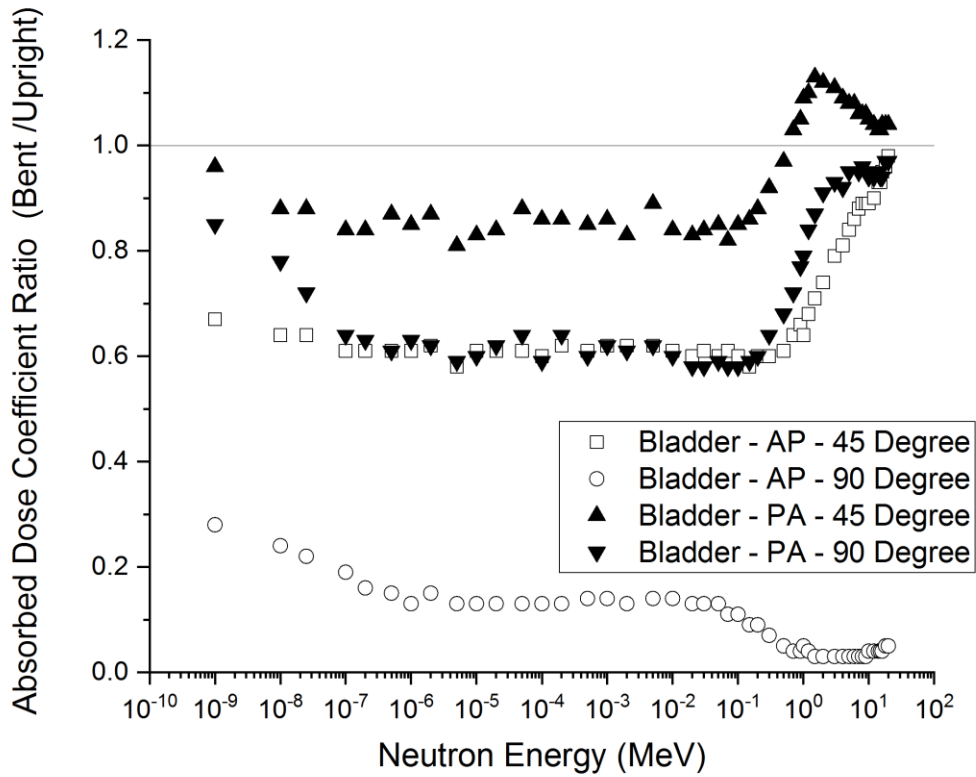
494  
495  
496



497  
498 **Fig 2** Neutron weighting factor,  $w_R$ , as a function of neutron energy, shown for energies  $1.0 \cdot 10^9$   
499 – 20 MeV.



501  
 502 **Fig 3** Sex-averaged absorbed dose coefficient ratio for brain in AP and PA irradiation  
 503 geometries with PIMAL bent at 45° and 90° postures. A horizontal line for a ratio of 1.0 is  
 504 provided as a visual reference for the reader.



506

507

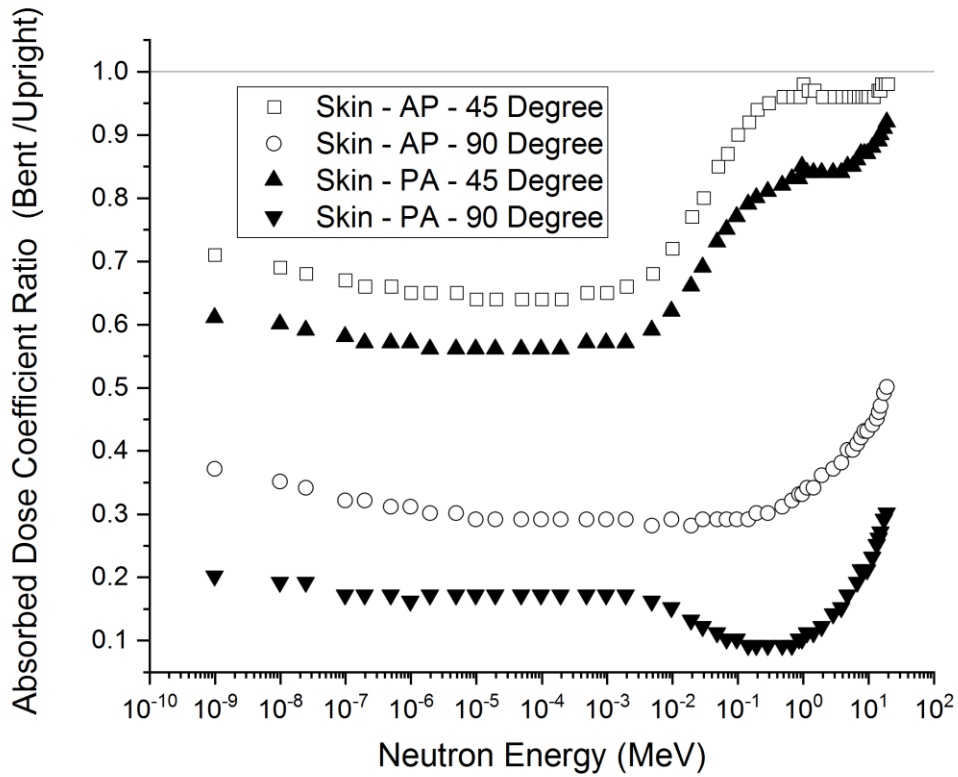
508

509 **Fig 4** Sex-averaged absorbed dose coefficient ratio for urinary bladder in AP and PA irradiation

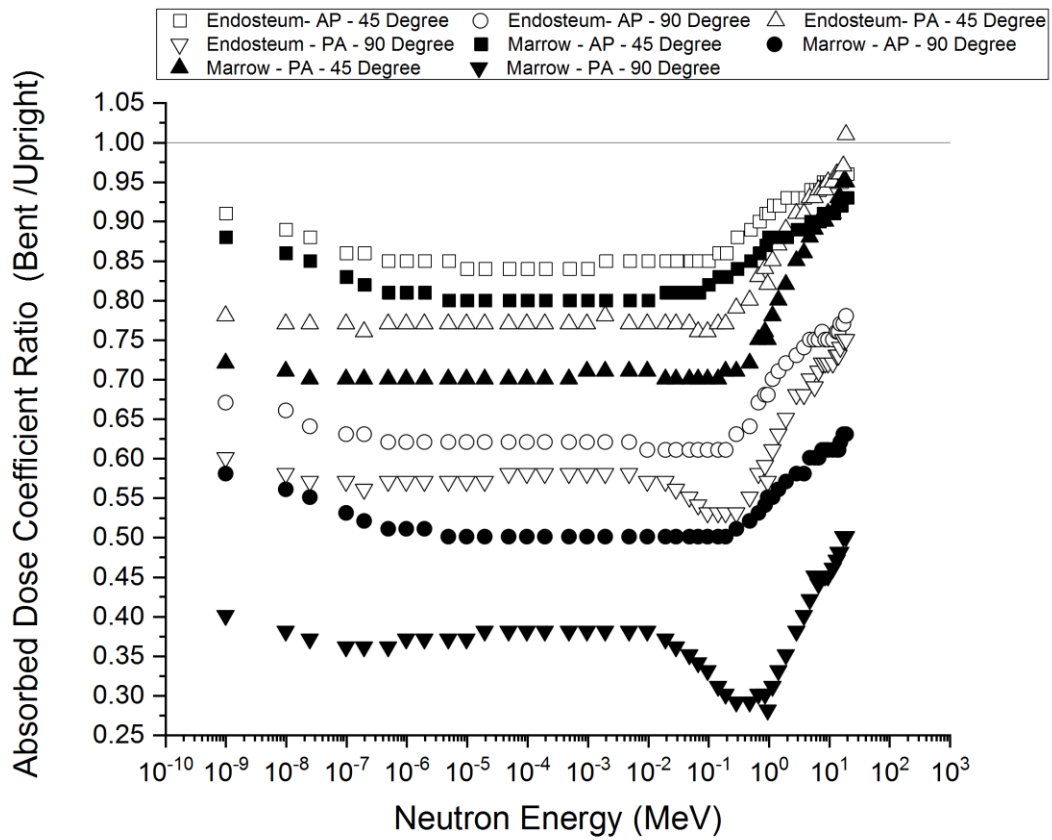
510 geometries with PIMAL bent at 45° and 90° postures. A horizontal line for a ratio of 1.0 is

511 provided as a visual reference for the reader.



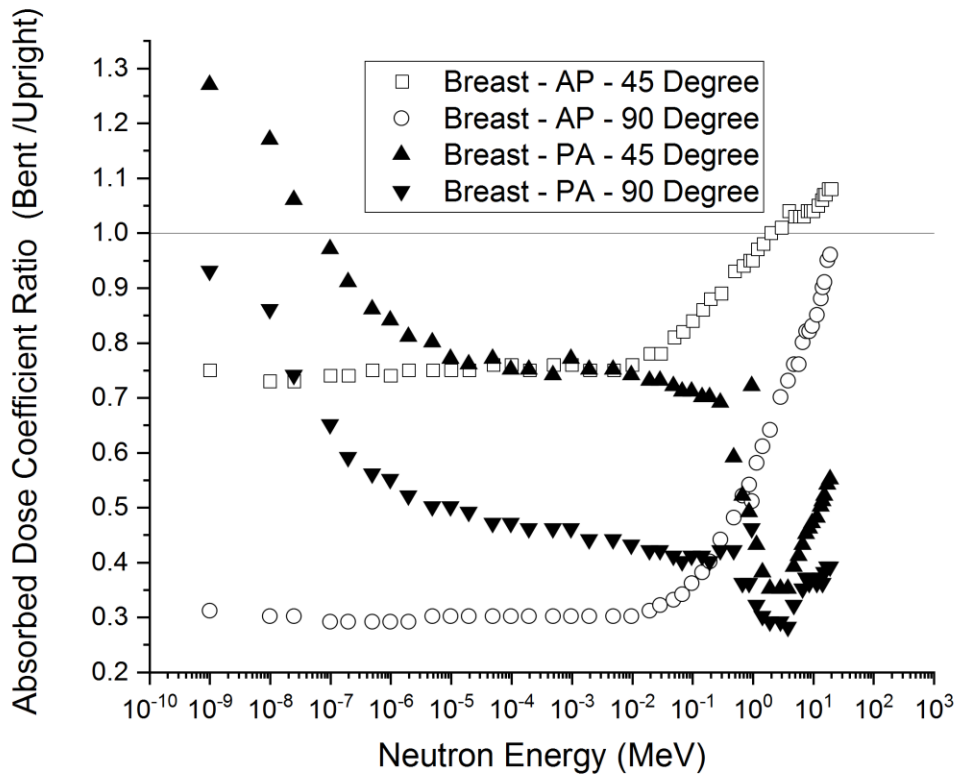


513  
 514 **Fig 5** Sex-averaged absorbed dose coefficient ratio for skin in AP and PA irradiation geometries  
 515 with PIMAL bent at 45° and 90° postures. A horizontal line for a ratio of 1.0 is provided as a  
 516 visual reference for the reader.

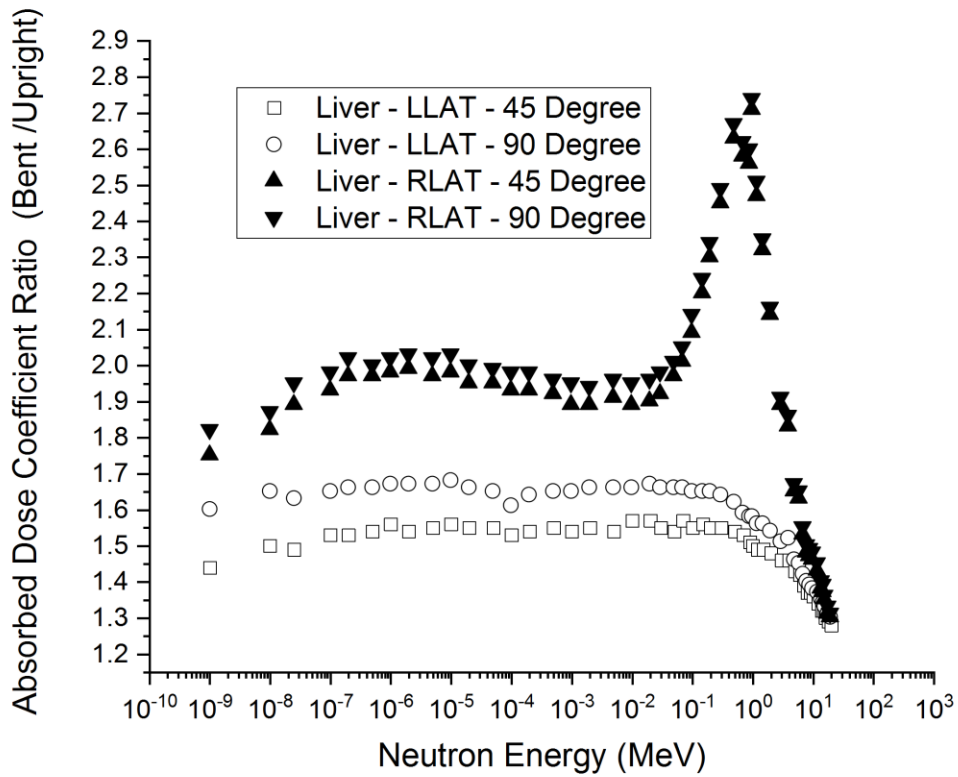


518  
 519  
 520  
 521

*Fig 6 Sex-averaged absorbed dose coefficient ratio for endosteum and active marrow in AP and PA irradiation geometries with PIMAL bent at 45° and 90° postures. A horizontal line for a ratio of 1.0 is provided as a visual reference for the reader.*

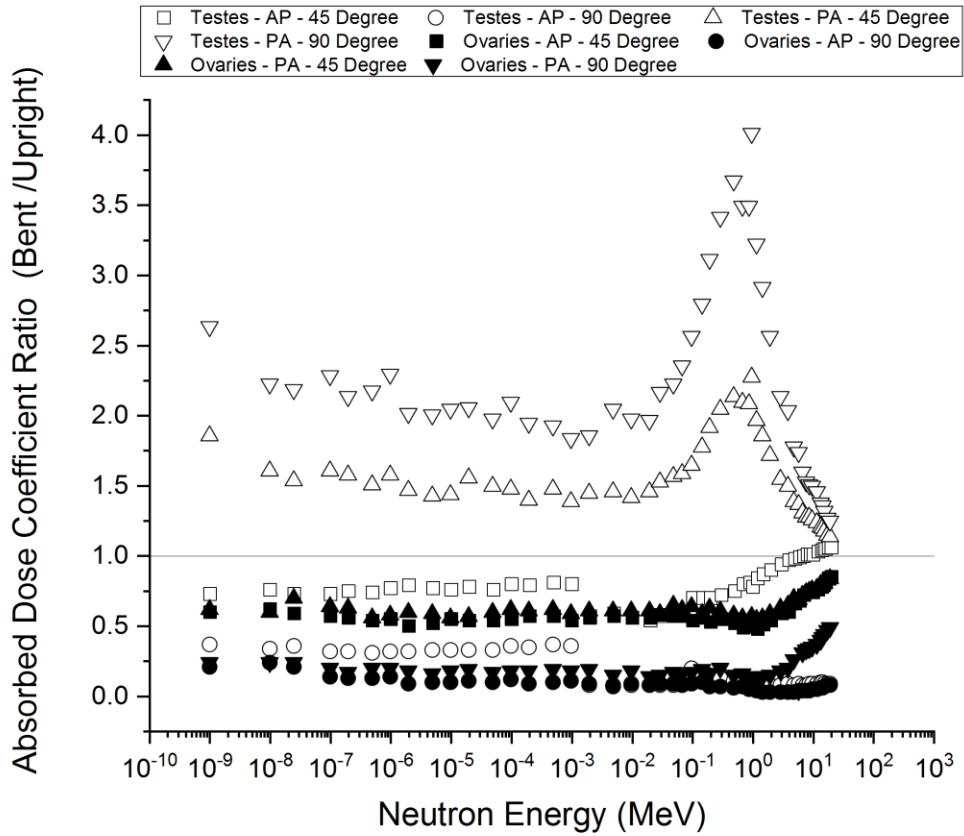


522  
 523 **Fig 7** Sex-averaged absorbed dose coefficient ratio for breast in AP and PA irradiation  
 524 geometries with PIMAL bent at 45° and 90° postures. A horizontal line for a ratio of 1.0 is  
 525 provided as a visual reference for the reader.



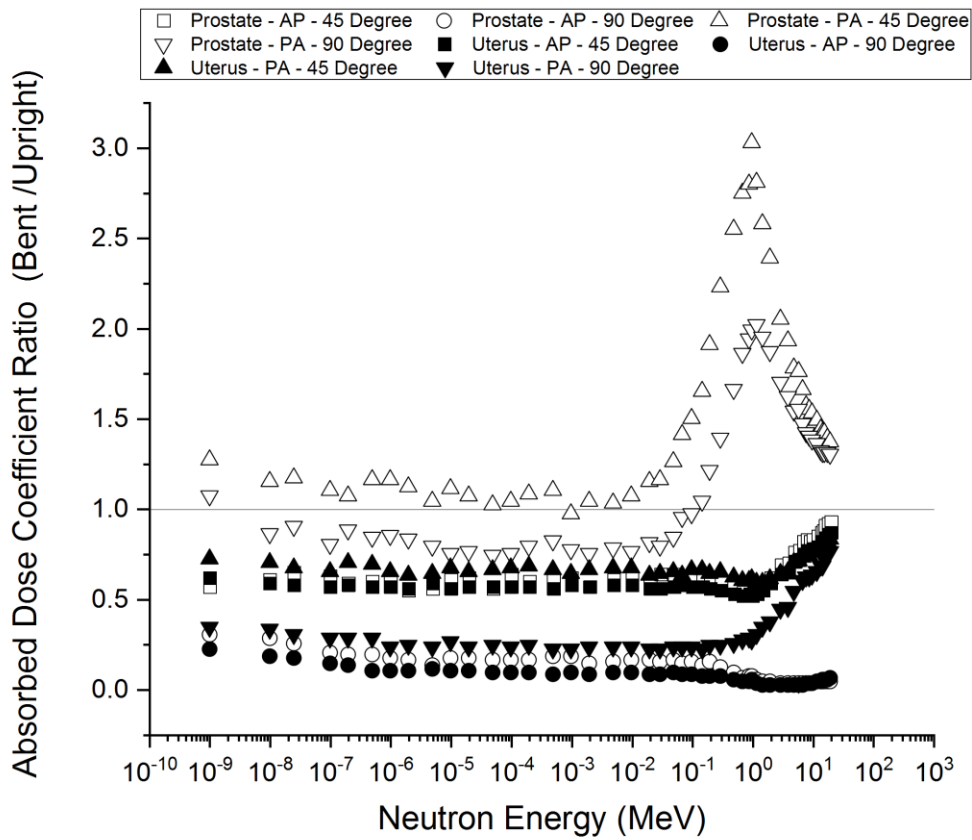
526  
 527  
 528

**Fig 8** Sex-averaged absorbed dose coefficient ratio for liver in LLAT and RLAT irradiation geometries with PIMAL bent at 45° and 90° postures.



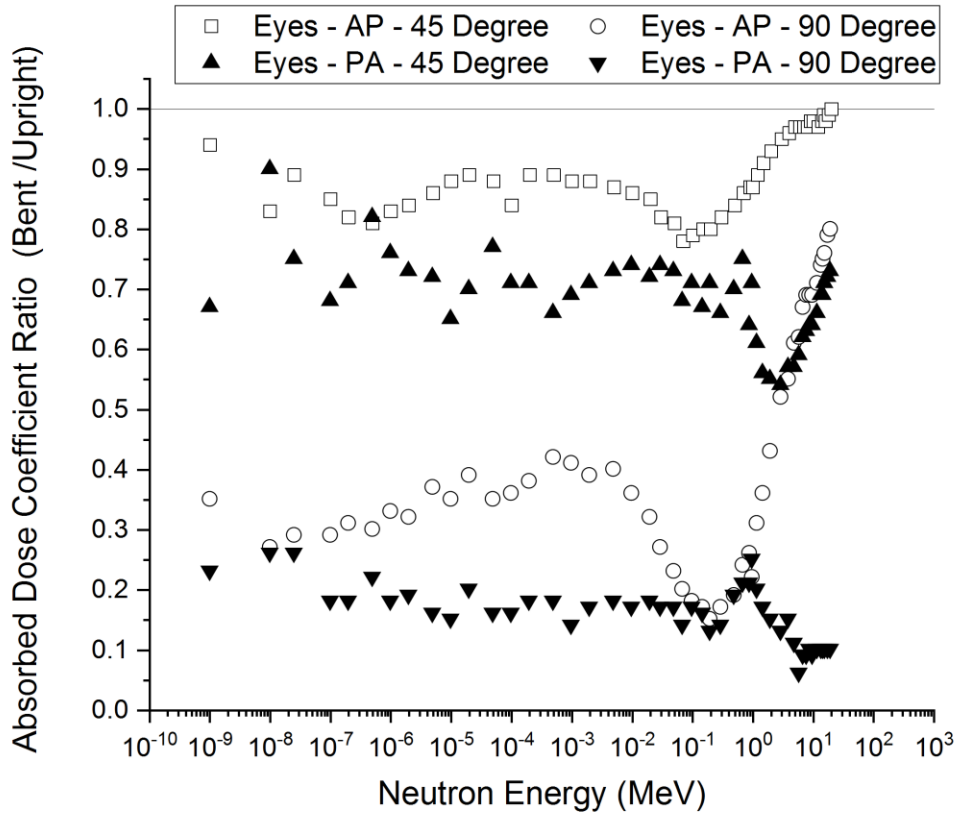
529  
 530  
 531  
 532

**Fig 9** Absorbed dose coefficient ratio for gonads (male: testes; female: ovaries) in AP and PA irradiation geometries with PIMAL bent at 45° and 90° postures. A horizontal line for a ratio of 1.0 is provided as a visual reference for the reader.



534  
 535  
 536  
 537

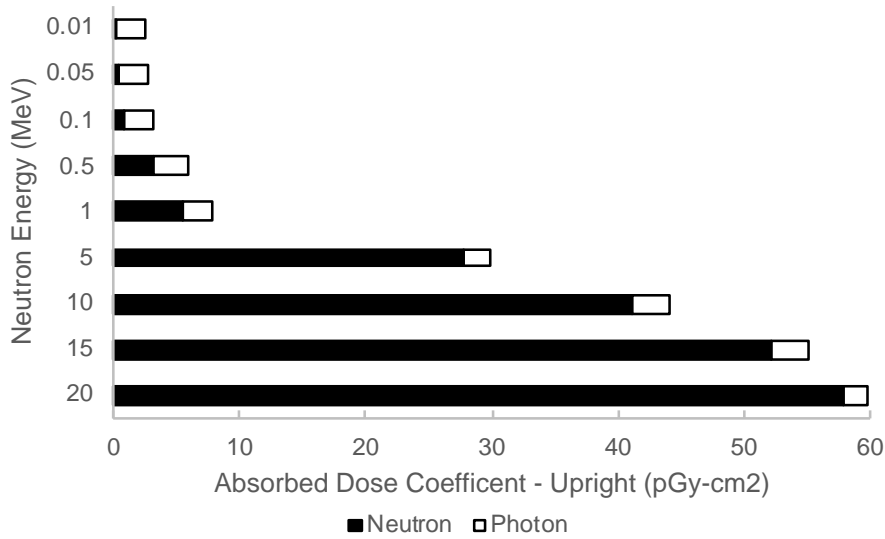
**Fig 10** Absorbed dose coefficient ratio for sex-specific organs (male: prostate; female: uterus) in AP and PA irradiation geometries with PIMAL bent at 45° and 90° postures. A horizontal line for a ratio of 1.0 is provided as a visual reference for the reader.



538  
 539 **Fig II** Sex-averaged absorbed dose coefficient ratio for eyes in AP and PA irradiation  
 540 geometries with PIMAL bent at 45° and 90° postures. A horizontal line for a ratio of 1.0 is  
 541 provided as a visual reference for the reader.

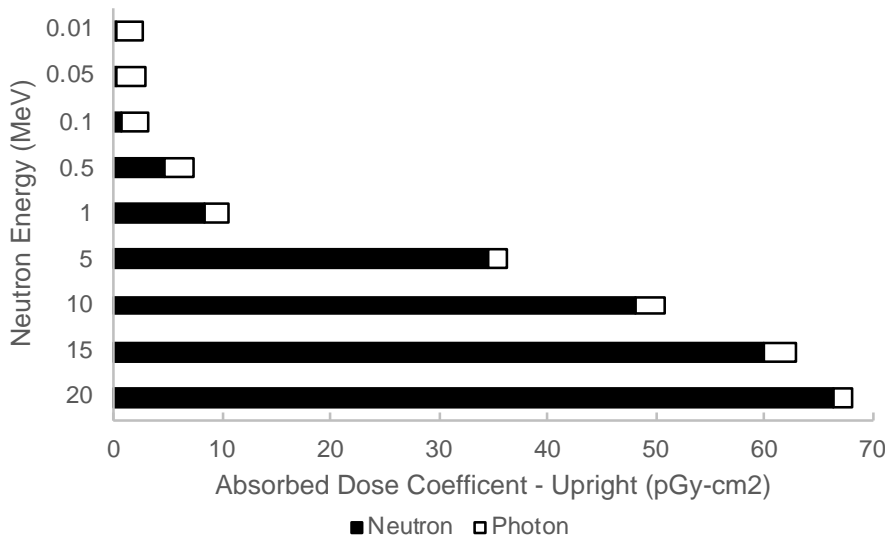
542

543



544  
545  
546

**Fig 12** Neutron and photon contributions to the absorbed dose coefficients for active marrow for selected energies in the AP irradiation geometry (upright male phantom).

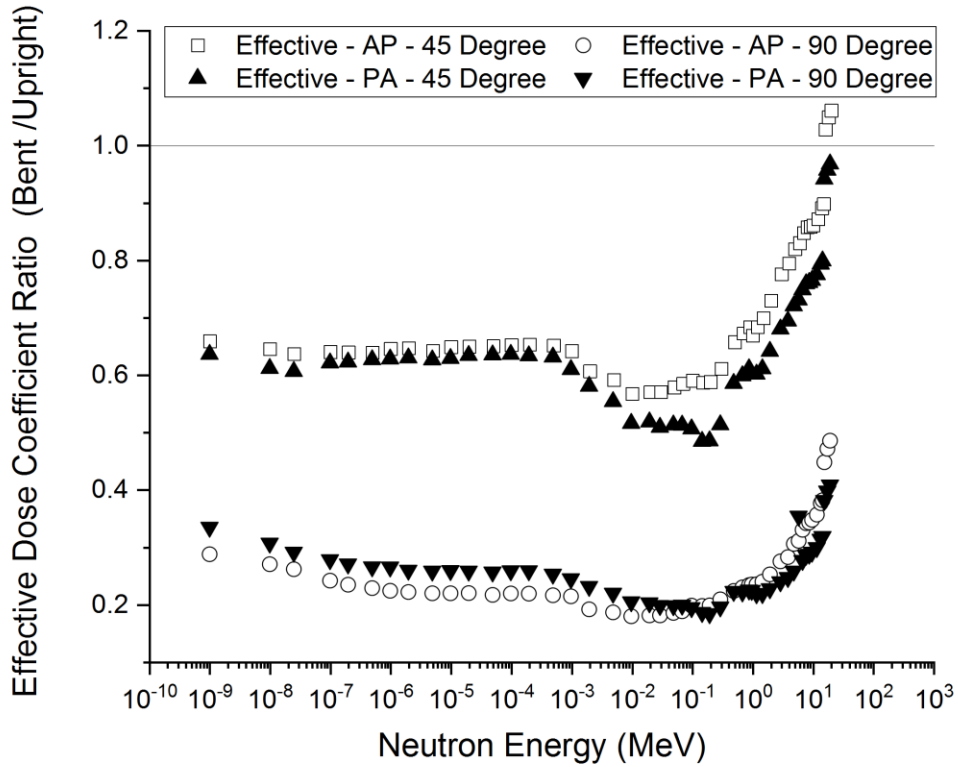


547  
548  
549

**Fig 13** Neutron and photon contributions to the absorbed dose coefficients for endosteum for selected energies in the AP irradiation geometry (upright male phantom).

550





551

552

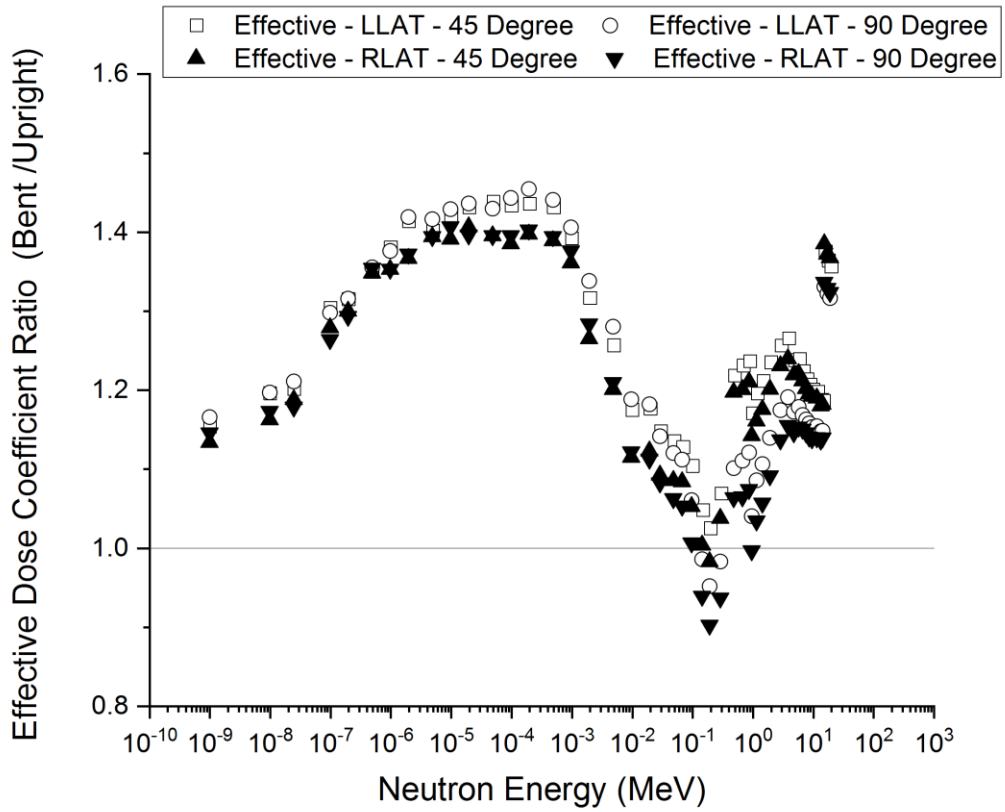
553 **Fig 14** Effective dose coefficient ratio in AP and PA irradiation geometries with PIMAL bent at  
 554 45° and 90° postures. A horizontal line for a ratio of 1.0 is provided as a visual reference for the  
 555 reader.

556

557

558

559



561  
 562 **Fig 15** Effective dose coefficient ratio in LLAT and RLAT irradiation geometries with PIMAL  
 563 bent at 45° and 90° postures. A horizontal line for a ratio of 1.0 is provided as a visual reference  
 564 for the reader.

565

566